Specialized germline P-bodies are required to specify germ cell fate in *C. elegans* embryos

Authors: Madeline Cassani and Geraldine Seydoux[1]

HHMI and Dept. of Molecular Biology and Genetics, Johns Hopkins University School of Medicine, Baltimore MD USA

1. Corresponding author: gseydoux@jhmi.edu

ABSTRACT

In animals with germ plasm, specification of the germline involves "germ granules", cytoplasmic condensates that enrich maternal transcripts in the germline founder cells. In *C. elegans* embryos, P granules enrich maternal transcripts, but surprisingly P granules are not essential for germ cell fate specification. Here we describe a second condensate in the *C. elegans* germ plasm. Like canonical P-bodies found in somatic cells, "germline P-bodies" contain regulators of mRNA decapping and deadenylation and, in addition, the intrinsically-disordered proteins MEG-1 and MEG-2 and the TIS11-family RNA-binding protein POS-1. Embryos lacking *meg-1* and *meg-2* do not stabilize P-body components, miss-regulate POS-1 targets, miss-specify the germline founder cell, and do not develop a germline. Our findings suggest that specification of the germ line involves at least two distinct condensates that independently enrich and regulate maternal mRNAs in the germline founder cells.

Introduction

The germ plasm is a specialized cytoplasm found in the eggs of certain insects, nematodes and vertebrates that serves as a vehicle to segregate maternal proteins and RNAs to the nascent embryonic germline (Kulkarni and Extavour, 2017). Germ plasm assembly is a derived trait that arose independently several times in evolution as an alternative to the ancestral mode of germ cell fate specification by cell-to-cell signaling (Kemph and Lynch, 2022). A convergent characteristic of germ plasm in both vertebrate and invertebrate species is the presence of "germ granules", micron-size ribonucleoprotein assemblies that contain RNAs

coding for factors that promote germ cell development (Kulkarni and Extavour, 2017). Germ granules segregate with the germ plasm to the germline founder cells and are thought to contribute to their specification as primordial germ cells ("PGCs"). Germ granules were initially described using electron microscopy as mostly amorphous, electron-dense, micron-sized structures not surrounded by membranes (Arkov and Ramos, 2010). Fluorescence microscopy studies and proteomics in *Drosophila*, zebrafish, *Xenopus*, *C. elegans* and mice have revealed the presence of different types of condensates in germ cells, some with complex sub-structure (Gallo et al., 2008; Wang et al., 2014; Vo et al., 2019; Eichler et al., 2020; Wan et al., 2018; Uebel et al., 2020; Uebel et al., 2021; Roovers et al., 2018; Neil et al., 2021; Yang et al., 2022; Aravin et al., 2009). These studies have hinted that germ cells contain multiple condensates that compartmentalize different RNA-centered activities that collectively specify germ cell fate. For example, polar granules and founder granules are distinct granules in the germ plasm of *Drosophila melanogaster* that harbor mRNAs that need to be translated (polar granules) or degraded (founder granules) for proper germline development (Eichler et al., 2020). Here we demonstrate that the *C. elegans* germ plasm also contains two condensate types that make distinct contributions towards germ cell fate.

The first condensates to be described in the *C. elegans* germ plasm were named P granules for their segregation with P (posterior) blastomeres through a series of 4 asymmetric divisions that eventually give rise to the germline founder cell P_4 (Strome and Wood, 1982; Fig. 1E). P granules are scaffolded by the nematode-specific, RGG-domain proteins PGL-1 and PGL-3, which form dense liquid-like condensates *in vitro* and *in vivo* (Brangwynne et al., 2009; Hanazawa et al., 2011; Updike et al., 2011; Saha et al., 2016; Putnam et al., 2019). In zygotes, the PGL condensates become covered on their surface by nanoscale solid clusters assembled by a pair of paralogous and redundant intrinsically-disordered proteins MEG-3 and MEG-4. MEG-3/4 form an essential protective layer that controls the dynamics and asymmetric segregation of PGL condensates into the P blastomeres in part by reducing the surface tension of PGL condensates (Folkmann and Putnam, et al., 2021). MEG-3/4 also recruit maternal mRNAs to P granules. MEG-3 binds RNA *in vitro* and co-precipitates with ~500 maternal mRNAs in embryonic lysates, including the Nanos homologue *nos-2* and the predicted E3 ubiquitin ligase

Y51F10.2 that are required redundantly for fertility (Lee et al., 2020). Incorporation into P granules enriches RNAs in the P_4 blastomere as much as 5-fold over what would have been achieved by equal segregation to all embryonic cells (Schmidt et al., 2021). *nos-2* and *Y51F10.2* are translationally repressed in the P_0 to P_3 blastomeres and become translationally activated in P_4, the germline founder cell (Subramaniam and Seydoux, 1999; Lee et al., 2020). Despite their role in enriching mRNAs required for germ cell development, P granules are not essential for germ cell fate. In *meg-3 meg-4* mutants, the germline founder cell P_4 inherits no PGL condensates and reduced levels of *nos-2* and *Y51F10.2* transcripts (Lee et al., 2020; Schmidt et al., 2021). These transcripts, however, are still translationally activated in P_4, and *meg-3 meg-4* animals are mostly (~70%) fertile (Lee et al., 2020). These observations indicate that the *C. elegans* germ plasm maintains proper regulation of maternal mRNAs in the absence of P granules.

The *C. elegans* germ plasm contains a second condensate type that contains proteins characteristic of P-bodies, ubiquitous RNP granules implicated in mRNA storage and decay (Gallo et al., 2008; Ivanov et al., 2019). P-body-like condensates associate with P granules in germ plasm in tight assemblies containing a central P granule surrounded by several P-body-like condensates (Gallo et al., 2008). Dozens of proteins have been reported to enrich in granules in the *C. elegans* germ plasm (Updike and Strome, 2010; Phillips and Updike, 2022), and, in most cases, it is not known whether these localize to P granules proper (as defined by PGL-3 and MEG-3) or to the closely apposed P-body-like condensates described in Gallo et al. 2008, or to both. In particular, MEG-1 and MEG-2 are two intrinsically-disordered proteins, distantly related to MEG-3 and MEG-4, and originally described as P granule proteins (Leacock and Reinke, 2008). In this study, we demonstrate that MEG-1 and MEG-2 associate with canonical P-body proteins and stabilize P-body-like condensates in P_4. Our findings indicate that, unlike P granules, "germline P-bodies" are essential for maternal mRNA regulation and specification of P_4 as the germline founder cell.

Results

MEG-1 enriches in puncta distinct from P granules

To characterize the localization of MEG-1, we used a MEG-1::GFP fusion where GFP is inserted at the C-terminus of the MEG-1 ORF in the *meg-1* locus. Consistent with a previous report that used a polyclonal antibody raised against MEG-1 (Leacock and Reinke, 2008), MEG-1::GFP segregated with germ plasm in early embryos, distributing between a cytoplasmic pool and bright puncta in P blastomeres that overlapped with P granules (Fig. 1A). High resolution images revealed that the MEG-1 puncta localize to the periphery of P granules (visualized with PGL-3 or MEG-3) in P_1 blastomeres (Fig. 1C,D, Fig. S1A). By the P_4 stage, when P granules are fully perinuclear, the MEG-1::GFP signal was distributed throughout P granules (Fig. 1C,D, Fig. S1A). In Z2 and Z3, MEG-1::GFP dispersed back into the cytoplasm (Fig. S1B) and turned over by mid-embryogenesis (Leacock and Reinke, 2008).

Leacock and Reinke, 2008 reported that MEG-1 enrichment in P blastomeres is independent of P granule components and vice versa. Consistent with these results, we found that MEG-1 still enriched preferentially in P blastomeres in *meg-3(ax3055) meg-4(ax3052)* mutants (Fig. 1B). MEG-1 puncta, however, remained cytoplasmic and did not associate with the nuclear envelope in P_4 of *meg-3(ax3055) meg-4(ax3052)* mutants (Fig. 1A-B). Leacock and Reinke, 2008 used a partial deletion of the *meg-1* locus and RNAi of the *meg-1* paralog *meg-2* to generate embryos depleted of both *meg-1* and *meg-2*. To complement these analyses, we created a deletion that removed the entire *meg-1 meg-2* operon. *meg-1 meg-2(ax4532)* hermaphrodites were 100% maternal effect sterile as reported for *meg-1(vr10) meg-2(RNAi)* (Table S1). We found that MEG-3 and PGL-3 still assembled into puncta that segregated with P blastomeres in *meg-1 meg-2(ax4532)* embryos, confirming that P granule assembly does not require *meg-1* and *meg-2* (Fig. S1C). We noticed, however, that P granule enrichment in P blastomeres was not as robust in *meg-1 meg-2* embryos (Fig. S1D) as previously reported (Leacock and Reinke, 2008; Wang et al., 2014), suggesting a minor contribution of MEG-1/2 to P granule segregation.

We conclude that MEG-1 localizes to assemblies that are distinct from P granules. MEG-1 puncta and P granules interact but assemble independently in the cytoplasm of P blastomeres.

117

118 *MEG-1 immunoprecipitates with P-body components and several RNA-binding proteins,*
119 *including POS-1*

120 As we show here for MEG-1, we previously reported that P-body markers enrich at the
121 periphery of P granules in early P blastomeres (Gallo et al., 2008). Furthermore, Wu et al., 2017
122 identified MEG-1 and MEG-2 among immunoprecipitates of the P-body scaffold C-NOT1^{NTL-1} and
123 identified seven CCR4-NOT subunits in MEG-2 immunoprecipitates. To complement these
124 studies, we performed mass spectrometry on MEG-1::GFP immunoprecipitated from early
125 embryo lysates using anti-GFP antibodies. As controls, we used lysates from wild-type worms
126 expressing untagged MEG-1. We identified 54 proteins that were enriched at least twofold over
127 untagged controls in two biological replicates (Fig. 2A, Table S2).

128 Among the proteins in MEG-1::GFP immunoprecipitates, we observed an enrichment for
129 canonical P-body proteins (7 out of 36 canonical P-body proteins in the *C. elegans*
130 genome/WormBase, $p<0.0001$, Fisher's exact test), including the decapping factors DCP2^{DCAP-2}
131 and EDC4^{EDC-4}, the TRIM-NHL family member and miRISC cofactor TRIM45^{NHL-2}, the CCR4-NOT
132 complex subunits CNOT1^{NTL-1}, CNOT2$^{TAG-153}$, CNOT3^{NTL-3} and the translational repressor and
133 DDX6-binding partner eIF4-ET^{IFET-1} (Table S2). In addition to P-body proteins, we also observed
134 eight RNA-binding proteins including the translational repressor GLD-1, the poly-A polymerase
135 GLD-2/GLD-3, the zinc finger proteins MEX-1, OMA-1 and POS-1, the KH domain protein MEX-3,
136 and the RRM domain protein SPN-4. All of these have been reported to regulate maternal
137 mRNAs and to enrich in germ plasm and "P granules" (because P-bodies and P granules are
138 closely linked in wild-type embryos, most studies have not distinguished between the two).
139 Among these, POS-1 scored as one of the most highly enriched proteins in MEG-1::GFP
140 precipitates after MEG-1 and MEG-2 (Fig. 2A, Table S2).

141 POS-1 regulates the poly-adenylation of thousands of maternal mRNAs containing AU-
142 rich elements (AREs) in their 3'UTR (Farley et al., 2008; Elewa et al., 2015). ARE-binding proteins
143 have been reported to recruit P-body components, including decapping enzymes and the
144 deadenylation machinery (Ciais et al., 2013). To confirm the interaction between POS-1 and
145 MEG-1, we probed the MEG-1::GFP immunoprecipitates with a polyclonal serum against POS-1

(Barbee and Evans, 2006) (Fig. 2B). This experiment confirmed that MEG-1::GFP precipitates contain POS-1, but not the control protein tubulin (Fig. 2B and Fig. S2A,B). POS-1 was not immunoprecipitated by a MEG-3::GFP fusion, further confirming the specificity of the MEG-1-POS-1 interaction (Fig. 2C and Fig. S2C,D). We conclude that MEG-1 exists in a complex that contains P-body components and RNA-binding proteins, including POS-1, a protein predicted to recruit P-body proteins to maternal mRNAs.

MEG-1 and POS-1 co-localize in P-body-like puncta in P_4

To examine the distribution of POS-1 and P-body components relative to MEG-1 and P granules, we used antibodies against POS-1 (Barbee and Evans, 2006) and P-body marker $DDX6^{CGH-1}$ (Alessi et al., 2015) and a mNeonGreen::3xFLAG fusion to P-body marker EDC-3 (abbreviated mNG::EDC-3, DeMott et al., 2021). In P_1 blastomeres, POS-1, $DDX6^{CGH-1}$ and EDC-3 enriched in condensates at the periphery of PGL-3 puncta (Fig. S3A). The POS-1, $DDX6^{CGH-1}$ and EDC-3 condensates overlapped but were not perfectly coincident with MEG-1 (Fig. S3B). In P_4, MEG-1, POS-1, $DDX6^{CGH-1}$ and EDC-3 appeared to mix more extensively with each other and PGL-3 (Fig. S3A,B). We reasoned that if P-body components associate with MEG-1, they might still form condensates in the absence of P granules. As expected, we found that in *meg-3 meg-4* embryos, which lack P granules, POS-1, $DDX6^{CGH-1}$ and EDC-3 enriched in cytoplasmic puncta most prominently in P_4, and these co-localized with MEG-1 (Fig. 3A).

C. elegans mRNAs can be detected using an oligo-dT probe that detects poly-adenylated mRNAs and a probe against SL1, the splice leader found on the 5' end of ~60% of *C. elegans* mRNAs (Seydoux and Fire, 1994). Consistent with enriching maternal mRNAs, P granules are positive for both SL1 and poly-A (Seydoux and Fire, 1994). We reasoned that, since P-bodies are thought to enrich deadenylated mRNAs (Ivanov et al., 2019), P-bodies might be positive for SL1 but not poly-A. P-bodies also assemble in somatic blastomeres, becoming most prominent at the 4-cell stage when degradation of maternal mRNAs begins in somatic lineages (Gallo et al., 2008). Consistent with harboring deadenylated mRNAs, somatic P-bodies marked by EDC-3 showed a high SL1 signal but no poly-A enrichment (compared to the surrounding cytoplasm, Fig. S3C). Similarly, we found that MEG-1::GFP puncta in P_4 of *meg-3 meg-4* embryos were

positive for SL1 but not poly-A (Fig. 3B). Interestingly, MEG-1::GFP puncta in P_3 were positive for both SL1 and poly-A (Fig. 3B), suggesting that at this stage MEG-1 puncta do not yet correspond to mature P-body-like structures.

Taken together, these observations suggest that, in early P blastomeres, MEG-1 and P-body proteins form overlapping, but not perfectly coincident, assemblies at the periphery of P granules. In P_4, MEG-1 and P-body components come together into condensates that contain deadenylated mRNAs. We refer to these P_4-specific condensates as "germline P-bodies" to distinguish these from somatic P-bodies which form in somatic blastomeres and do not contain MEG-1 or POS-1.

meg-1 and meg-2 are required to maintain DDX6^{CGH-1} and EDC-3 and assemble robust germline P-bodies in P_4.

Unlike P granule proteins, such as PGL-3, which are asymmetrically segregated from the zygote stage (Fig. S1D), DDX6^{CGH-1} and EDC-3 are inherited by all blastomeres during early cleavages. After the 8-cell stage, DDX6^{CGH-1} is turned over in somatic blastomeres (Boag et al., 2005) and remains at high levels only in P_4 (Fig. S4A-C). EDC-3 is maintained in somatic blastomeres throughout embryogenesis but enriches in P_4 (Fig. S4D-F). In *meg-1 meg-2* mutants, DDX6^{CGH-1} and EDC-3 distributions were unchanged through the 8-cell stage, but DDX6^{CGH-1} was not maintained, and EDC-3 was not enriched, in P_4 (Fig. S4). In contrast, POS-1, which enriches with germ plasm from the zygote stage (Han et al., 2018), was not affected in *meg-1 meg-2* (Fig. 4A). To quantify these observations, we compared the levels in P_4 of DDX6^{CGH-1}, EDC-3 and POS-1 in *meg-1 meg-2*, *meg-3 meg-4*, and embryos depleted of all four MEG proteins [*meg-1(vr10) meg-2(RNAi) meg-3(tm4259) meg-4(RNAi)* embryos] (Fig. 4A). DDX6^{CGH-1} and EDC-3 levels were significantly reduced in P_4 of *meg-1 meg-2* embryos compared to wild-type and in *meg-1 meg-2 meg-3 meg-4* embryos compared to *meg-3 meg-4* embryos (Fig. 4A,B). In contrast, POS-1 levels were not significantly affected in either *meg-1 meg-2* or *meg-3 meg-4* mutants and were reduced only in the quadruple mutant. We conclude that MEG-1/2 are essential to maintain high levels of DDX6^{CGH-1} and EDC-3 in P_4 and are required redundantly with MEG-3/4 to maintain high levels of POS-1 in P_4.

The reduction in DDX6^{CGH-1} and EDC-3 levels in P_4 suggests that germline P-body activity might be compromised in *meg-1 meg-2* mutants. Consistent with this hypothesis, *in situ* hybridization against poly-A and SL1 revealed that poly-A levels were higher in P_4 of *meg-1 meg-2* embryos compared to wild-type and in *meg-1 meg-2 meg-3 meg-4* embryos compared to *meg-3 meg-4* embryos, despite either a reduction or no significant change in SL1 levels (Fig. 4C,D). We observed SL1+ puncta in P_4 in 14/17 of *meg-3 meg-4* embryos and in 4/20 *meg-1 meg-2 meg-3 meg-4* embryos (Fig. S5A). The SL1+ puncta did not enrich poly-A over the cytoplasm in *meg-3 meg-4* embryos but did in *meg-1 meg-2 meg-3 meg-4* embryos (Fig. S5A). Together these observations indicate that MEG-1 and MEG-2 are required to maintain robust levels of P-body proteins and robust activation of mRNA deadenylation in P_4.

meg-1 meg-2 embryos fail to turnover transcripts targeted for deadenylation by POS-1

To examine directly whether *meg-1 meg-2* mutants exhibit defects in maternal mRNA regulation, we performed RNAseq to compare the transcriptomes of *meg-1 meg-2* mutant embryos to that of wild-type. Two independent RNA-seq libraries were analyzed for each genotype (wild type and *meg-1(vr10) meg-2(RNAi)*). This analysis identified 550 upregulated mRNAs, and 230 downregulated mRNAs, in *meg-1 meg-2* embryos compared to wild-type (±1.5 fold change, $p<0.05$; Fig. 5A, Table S3).

Elewa et al., 2015 identified 3,726 transcripts that display longer poly-A tails in *pos-1*(RNAi) embryos compared to wild-type ("deadenylated POS-1 targets"), of which 3,718 were detected in our RNA-seq. 40% of genes (223/550) upregulated in *meg-1 meg-2* embryos were among these deadenylated POS-1 targets (Fig. 5B, Table S3). Assuming a total pool of 11,121 transcripts that can be detected by these analyses in early embryos (see Methods), we found this overlap to be significant (Fisher's exact test, p-value=0.0002). In comparison, the overlap between transcripts downregulated in *meg-1 meg-2* embryos and deadenylated POS-1 targets (30/3,718 transcripts; p-value = 1) or adenylated POS-1 targets (transcripts with shorter poly-A tails in *pos-1*(RNAi); 17/1,307; p-value=0.99) was not significant (but see next section). We conclude that MEG-1 and MEG-2 contribute to the turn-over of a subset of maternal mRNAs also targeted by POS-1 for deadenylation.

neg-1 and *cdc-25.3* are two transcripts among the 223 potential targets shared between POS-1 and MEG-1. *neg-1* and *cdc-25.3* are maternally-deposited and turned over in all lineages by the 28-cell stage (Fig. S6A,B; Tintori et al., 2016; Elewa et al., 2015). In *meg-1 meg-2* embryos, but not in *meg-3 meg-4* embryos, *neg-1* and *cdc-25.3* transcripts were still detected in P_4 in the 28-cell stage (Fig. 5C-F and Fig. S6C,D). These observations confirm that *meg-1/2* activity is required for the efficient turnover of a subset of POS-1-regulated transcripts.

meg-1 meg-2 embryos fail to express efficiently transcripts activated by POS-1 for translation in P_4

In addition to promoting deadenylation of a subset of maternal transcripts, POS-1 is also required to extend the poly-A tail of a different group of maternal transcripts that are translationally activated in embryos, including *nos-2, Y51F10.2* and *xnd-1* (Elewa et al., 2015). These transcripts code for factors required for germ cell fate and are translationally repressed in the P_0, P_1, P_2 and P_3 blastomeres and translationally activated in P_4 (Lee et al. 2020; Mainpal et al., 2015). Translational activation of *nos-2* and *Y51F10.2* has been confirmed to require POS-1 (D'Agostino et al., 2006; Jadhav et al., 2008; Lee et al., 2020).

We used *in situ* hybridization and immunofluorescence to examine transcript and protein levels in P_4 of wild type, *meg-1 meg-2*, *meg-3 meg-4* and *meg1 meg-2 meg-3 meg-4* embryos (Fig. 6). We found that for all three transcripts, RNA levels were lowest in the *meg-3 meg-4* mutants, consistent with a dependence on P granules for enrichment in P_4. RNA levels were also reduced in *meg-1 meg-2* mutants compared to wild-type, suggesting that MEG-1/2 also contribute to RNA enrichment either directly or indirectly through an effect on P granule segregation, since P granules are also inefficiently segregated in these mutants (Fig. S1D). Adjusting for RNA levels, we found that protein output was reduced in *meg-1 meg-2* and elevated in *meg-3 meg-4* compared to wild-type (Fig. 6). These differences did not correlate with POS-1 protein levels in P_4, which were similar in these mutants (Fig. 4 A,B). Consistent with *meg-1 meg-2* and *meg-3 meg-4* acting in parallel, protein levels were lowest in embryos depleted of all four *meg*s compared to either double combination. Together, these observations suggest that *meg-1 meg-2* and *meg-3 meg-4* contribute independently to

expression of maternal transcripts in P_4, with MEG-3/4 acting primarily by boosting RNA levels and MEG-1/2 primarily by boosting protein output.

In wild type, *nos-2* and *Y51F10.2* RNAs enrich in P granules through P_3 and become cytoplasmic in P_4 coincident with translational activation (Lee et al., 2020). [*xnd-1* is a much less abundant transcript which precluded us from evaluating its partitioning between P granules and the cytoplasm (Fig. 6E)]. Consistent with reduced translational activation in P_4, we observed that *nos-2* and *Y51F10.2* remained enriched in a perinuclear pattern in *meg-1 meg-2* embryos, as also observed in *pos-1* embryos (Lee et al., 2020) (Fig. 6A,C, Fig. S7). As mentioned above, *nos-2* and *Y51F10.2* exhibited a higher protein output in P_4 in *meg-3 meg-4* embryos compared to wild-type and *meg-1 meg-2* embryos (Fig. 6B and 6D), suggesting that assembly into P granules dampens translational activation. We could not determine translational output in *meg-1 meg-2 meg-3 meg-4* due to the extremely low levels of RNA in P_4 in these mutants. We conclude that *meg-1 meg-2* are required for maximal translation activation of POS-1 targets in P_4, which is antagonized by *meg-3 meg-4*.

Primordial germ cells adopt a muscle precursor-like cell fate in meg-1 meg-2 mutants

In *pos-1* mutants, P_4 descendants develop as muscle precursor cells that express the myoD homolog *hlh-1* (Tabara et al., 1999). To determine whether a similar cell fate transformation occurs in *meg-1 meg-2* mutants, we examined the expression of *hlh-1* and the PGC zygotic transcript *xnd-1* (Mainpal et al., 2015) by *in situ* hybridization using a P granule marker to identify P_4 descendants. We observed *hlh-1* transcripts in P_4 descendants in 21/23 bean to comma stage *meg-1 meg-2* embryos examined, compared to 0/21 wild-type embryos examined (Fig. 7A). In contrast, we failed to observe robust expression of *xnd-1* in 16/24 *meg-1 meg-2* embryos (Fig. 7B).

In wild type, the daughters of P_4 (Z2 and Z3) remain non-proliferative during embryogenesis and only divide in L1 larvae after the onset of feeding. In *meg-1 meg-2* mutants, we observed more than two P granule-positive cells in 50% of bean-to-comma cell stage embryos (Fig. 7C) and in 100% of non-fed L1 larvae stage (Fig. 7D). The extra P granule-positive cells were not due to miss-segregation of P granules to the D blastomere (Fig. S8A), were first

detected around the 35-45 cell stage (Fig. S8B) and did not express muscle myosin (Fig. S8C). We conclude that primordial germ cells are partially transformed to muscle precursor-like fate in *meg-1 meg-2* mutants.

The *meg-1 meg-2* phenotype contrasts with that of *meg-3 meg-4* embryos where Z2 and Z3 express *xnd-1*, do not express *hlh-1* and do not proliferate prematurely despite the absence of maternal P granules (Fig. 7A,B; Wang et al., 2014). ~70% of *meg-3 meg-4* mutants are fertile, in contrast to *meg-1 meg-2* mutants which are 100% sterile (Leacock and Reinke et al., 2008; Wang et al., 2014).

Discussion

In this study, we demonstrate that the germ plasm of *C. elegans* contains two condensate types, P granules and germline P-bodies. Each rely on a different pair of intrinsically-disordered proteins for efficient accumulation in the germline founder cell P_4: P granules depend on MEG-3 and MEG-4 and germline P-bodies depend on MEG-1 and MEG-2. We used these distinct genetic requirements to distinguish the contribution of each condensate to germ cell fate (Fig. 7E). P granules enrich regulators of small RNA homeostasis (Ouyang et al., 2019) and maternal mRNAs but are not required for maternal mRNA regulation (Lee et al, 2020 and this study). mRNA regulation depends on "germline P-bodies", which promote the translation of mRNAs coding for germline determinants and the turn-over of mRNAs coding for somatic determinants. We propose that the germ cell fate-specifying "germ granules" of *C. elegans* are assemblies of at least two distinct condensates, P granules and germline P-bodies, which enrich and regulate, respectively, maternal mRNAs in the germline founder cells.

Germline P-bodies and P granules are two types of condensates that require MEG proteins for stabilization in the embryonic germ lineage

P granules were the first characterized condensates in the *C. elegans* germ plasm (Strome and Wood, 1982). P granules consist of a dense liquid core, assembled by PGL proteins, surrounded by interfacial nanoscale, RNA-rich solid clusters assembled by intrinsically-disordered proteins MEG-3 and MEG-4 (Folkmann and Putnam et al., 2021). In this study, we

describe a second condensate type, germline P-bodies, that contains regulators of mRNA adenylation and decapping, the RNA-binding protein POS-1, and MEG-1 and MEG-2, two intrinsically-disordered proteins related to MEG-3 and MEG-4. Germline P-body components assemble in complex patterns around P granules in early P blastomeres and merge with each other and P granules in P_4. In embryos lacking P granules (*meg-3 meg-4* mutants), germline P-bodies can be visualized in P_4 as discrete SL1+ poly-A- cytoplasmic puncta that are also positive for MEG-1, POS-1 and the canonical P-body markers DDX6^{CGH-1} and EDC-3. In the absence of *meg-1 meg-2*, DDX6^{CGH-1} and EDC-3 levels are reduced and maternal mRNA regulation fails, despite normal P granule assembly and POS-1 levels (Fig. 7E).

How MEG-1/2 stabilize germline P-body components remains unclear. Unlike MEG-3/4 which are required for the asymmetric segregation of P granules from the zygote stage onward, MEG-1/2 do not appear to affect the distribution of germline P-body components until after the 8-cell stage. P-body components (DDX6^{CGH-1} and EDC-3) are initially segregated to all cells and coalesce into puncta in somatic cells coincident with the onset of maternal mRNA degradation (Gallo et al., 2008). MEG-1/2 do not affect P-body assembly in somatic cells but are required for stabilization of DDX6^{CGH-1} and EDC-3 specifically in P_4, at the embryonic stage when DDX6^{CGH-1} is rapidly cleared from somatic lineages. In *Drosophila* embryos, the DDX6/4-ET-like complex (ME31B/Cup) is targeted for degradation by CTLH, an E3 ubiquitin ligase, and Marie Kondo, an E2 conjugating enzyme (Cao et al., 2020; Zavortink et al., 2020). It will be interesting to determine whether homologs of these factors promote DDX6^{CGH-1} turnover in *C. elegans* and how MEG-1/2 might oppose these activities in P_4.

In contrast to somatic blastomeres which activate zygotic transcription by the 4-cell stage, P blastomeres remain transcriptionally silent until the birth of the daughters of P_4, the primordial germ cells Z2 and Z3 (100-cell stage). We suggest that MEG-enhanced condensation of P granules and germline P-bodies serves as a mechanism to concentrate maternally-provided mRNAs and their regulators in germ plasm to ensure that P_4 inherits sufficient machinery to initiate the maternal-to-zygotic transition. The MEG-1/2 and MEG-3/4 paralog pairs appear to have diverged such that MEG-1/2 interact preferentially with P-body components and MEG-3/4 interact preferentially with P granule components. MEG-3/4, but not MEG-1/2, contain an

HMG-like domain essential for MEG-3/4 clusters to associate with the surface of PGL condensates (Schmidt et al., 2021). MEG-3/4 stabilize PGL condensates by lowering their surface tension (Folkmann and Putnam et al., 2021); it remains to be determined whether MEG-1/2 function similarly or by another mechanism.

Germline P-body proteins control maternal mRNA regulation in the germline founder cell P_4

The birth of the P_4 blastomere appears to coincide with a major transition in maternal mRNA regulation in the P lineage as evidenced by 1) coalescence of germline P-bodies containing deadenylated mRNAs, 2) degradation of transcripts coding for somatic factors, and 3) translation of transcripts coding for germ cell fate determinants. We suggest that regulators of mRNA adenylation and decapping that enrich in P-bodies drive this transition in P_4 by targeting maternal mRNAs for de-adenylation/degradation or adenylation/translation, depending on the combination of RNA-binding proteins, including POS-1, bound to 3' UTRs. The poly-A polymerase subunits GLD-2 and GLD-3 are enriched in MEG-1 immunoprecipitates and have been reported to enrich in granules in germ plasm (Wang et al., 2002; Eckmann et al., 2002). It will be interesting to determine whether GLD-2/3 also localize to germline P-bodies and are responsible for the translational activation of transcripts like *nos-2*, *Y51F10.2* and *xnd-1*.

The birth of P_4 also coincides with the apparent mixing of germline P-bodies and P granules and the release of *nos-2* and *Y51F10.2* mRNAs from P granules coincident with their translational activation. This is also the stage where Z granules and SIMR-1 foci appear to de-mix from P granules to form the multi-condensate nuage characteristic of pre-gametic germ cells (Wan et al., 2018; Uebel et al., 2021). These observations suggest a dramatic switch in the material properties of condensates in the transition from P_3 to P_4. We do not know whether these changes arise as a cause, or consequence, of the changes in mRNA regulation that also occur at this stage. In principle, segregation of maternal mRNAs and their regulators into distinct condensates that eventually merge in P_4 could be used as a physical mechanism to control RNA-protein interactions. Alternatively, changes in condensation patterns could derive from changes in the composition and solubility of complexes dispersed throughout the cytoplasm. We favor the latter since 1) RNAs and proteins enriched in P granules and P-bodies

are also found dispersed throughout the cytoplasm and 2) failure to assemble P granules does not prevent timely translational regulation of mRNAs enriched in P granules. We suggest that the complex condensation patterns of germline P-body components in early P blastomeres, and apparent "mixing" with P granules in P_4, are mesoscale manifestations of molecular-scale rearrangements that occur throughout the cytoplasm and eventually culminate in the targeting of the P-body machinery onto maternal mRNAs in P_4. What regulates these changes during developmental time remains a mystery. The significance of the close association of germline P-bodies with P granules is also unclear and may reflect the fact that the two condensate types likely share some components such as POS-1, which depends on both MEG-1/2 and MEG-3/4 for maximal segregation to P_4 (Fig. 4B).

A conserved role for P-body proteins in specifying germ cell fate

In *meg-1 meg-2* mutants, P_4 descendants divide precociously, fail to activate the transcription of the germ cell transcript *xnd-1* and activate instead the transcription of the muscle transcription factor $MyoD^{HLH-1}$. These observations suggest a transformation to a muscle precursor fate, such as that normally adopted by the sister of P_4, the somatic blastomere D. This fate transformation occurs despite maintenance of P granules in Z2 and Z3 and their descendants, confirming that P granules are neither sufficient nor required to specify germ cell fate in primordial germ cells (Gallo et al., 2010; Strome et al., 1995). A similar $P_4 \rightarrow$ D fate transformation was reported for *pos-1* mutants (Tabara et al., 1999). The apparent $P_4 \rightarrow$ D fate transformation is likely incomplete as Z2 and Z3 descendants do not express muscle myosin, remain in their normal central position in embryos and first-stage larvae, and stall proliferation during the first larval stage. *meg-1 meg-2* fail to efficiently translate NOS-2 and Y51F10.2, two proteins implicated, respectively, in mRNA and protein turnover (Subramaniam and Seydoux, 1999; Kipreos, 2005). We showed previously that the sterility of embryos lacking Nanos could be rescued by reducing the activity of maternal LIN-15B, a soma-promoting transcription factor expressed in oocytes (Lee et al., 2017). Similarly, the germ cell proliferation defect of *meg-1 meg-2* larvae could be rescued partially by reducing *gld-1* activity (Kapelle and Reinke, 2011), an RNA-binding protein required for oocyte development and expressed in early P blastomeres

(Francis et al., 1995; Jones et al., 1996). Together these observations suggest that a key step to specify P_4 as the germline founder cell is to program germline P-bodies to eliminate maternal factors that function during oogenesis.

The germline P-bodies we describe here share several features with the recently described "founder granules" in *Drosophila* germ plasm. Founder granules contain DDX6^{ME31B}, the decapping factor DCP1 and Oskar mRNA, which although required for germ plasm assembly in oocytes, must be degraded in embryos for proper germline development (Eichler et al., 2020). DDX6^{ME31B} has been proposed to enrich in germ plasm independently of the canonical Oskar polar granule assembly pathway (McCambridge et al., 2020), as we demonstrate here for germline P-bodies, which assemble independently of P granules. Founder granules, however, have not yet been implicated in the translational activation of Nanos and other mRNAs enriched in polar granules, as we suggest here for germline P-bodies.

A role for P-bodies in early germ cell development has also been suggested by studies in mice. The mammalian Nanos homolog NANOS2 localizes to P-bodies, interacts with the CCR4-NOT1 deadenylation complex, and promotes mRNA degradation and the male germ cell fate program in mice (Suzuki et al., 2010; Shimada et al., 2019; Wright et al., 2021). DDX6/Me31B RNA helicases have also been implicated in the differentiation of various stem cell populations in human, mouse, and *Drosophila* (Di Stefano et al., 2019; Nicklas et al., 2015; Jensen et al., 2021). Together these studies suggest a conserved role for P-bodies as essential regulators of cell fate transitions in progenitors of the germline and beyond.

Limitations of the study

We inferred a requirement for P-body activity in embryonic germ cells through our analyses of *meg-1 meg-2* mutants which fail to stabilize germline P-bodies and regulate maternal mRNAs in P_4. We did not test directly, however, for a requirement for P-body enzymatic activity, as mutants in key P-body proteins arrest development before the birth of P_4. For example, RNAi reduction of the scaffold C-NOT1^{NTL-1} leads to early embryonic division defects, presumably because P-bodies also regulate the fate of mRNAs in somatic blastomeres (Gallo et al., 2008). The helicase DDX6^{CGH-1} stabilizes translationally repressed mRNAs during

oogenesis and is essential for the production of mature oocytes that support normal embryogenesis (Boag et al., 2008; Noble et al., 2008). A DDX6^{CGH-1} temperature-sensitive mutant is available (Scheckel et al., 2012), which could potentially allow us to bypass an earlier requirement for DDX6^{CGH-1}, but initial experiments proved inconclusive. Although we demonstrate that MEG-1 can be immunoprecipitated from lysates in a complex with POS-1 and a subset of P-body proteins, we have not investigated whether MEG-1 binds directly to these proteins or interacts indirectly by binding RNA for example. We also do not address whether MEG-1/2 or germline P-bodies are merely required (permissive) or are sufficient (instructive) to specify germ cell fate. MEG-1/2 enrich preferentially into P blastomeres from the zygote-stage onward; mutations that prevent this localization may help determine whether MEG-1/2 play a permissive or instructive role in germ cell fate specification.

Acknowledgments:

We thank John Kim and Amelia Alessi, Tom Evans, and Judith Yanowitz for the CGH-1, POS-1, and XND-1 antibodies; Dominique Rasoloson and Helen Schmidt for the MEG-1::GFP and MEG-1::OLLAS alleles; Tu Lu for the strains JH3472, JH3410, JH3404 and JH3352; the Johns Hopkins Microscope Facility (S10OD023548) for microscopy support; the Johns Hopkins University School of Medicine Genetic Resources Core Facility for sequencing support, and the JHMI Mass Spectrometry and Proteomics Facility for mass-spec support. We also thank the Seydoux lab and the Baltimore Worm Club for their insights during this project. Some strains were provided by the CGC, which is funded by NIH Office of Research Infrastructure Programs (P40 OD010440). Funding was provided by the National Institutes of Health (GS: R37HD037047; MC: T32 GM007445) and the National Science Foundation (MC: DGE-1746891). GS is an investigator of the Howard Hughes Medical Institute.

Competing Interests Statement

G.S. serves on the Scientific Advisory Board of Dewpoint Therapeutics, Inc. The remaining authors declare no competing interests.

Data availability

Sequencing data has been deposited onto the Gene Expression Omnibus (GEO) and can be found using the following accession numbers:

#########

Mass spectrometry data has been deposited to the MassIVE repository and can be found with the identifier #########.

Methods

Worm handling, RNAi, sterility counts

C. elegans were cultured according to standard methods (Brenner, 1974). Strains used in this study are listed in Table S4. RNAi knockdown experiments were performed by feeding on HT115 bacteria (Timmons and Fire, 1998). The empty pL4440 vector was used as a negative control. Bacteria were grown at 37°C in LB + ampicillin (100 µg/mL) media for 5 hours, induced with 5 mM IPTG for 30 minutes, plated on NNGM (nematode nutritional growth media) + ampicillin (100 µg/mL) + IPTG (1 mM) plates, and grown overnight at room temperature. L4 hermaphrodites were put onto RNAi plates and fed overnight at 25˚C, and then shifted back to 20˚C for at least one hour before proceeding with further experiments. Effectiveness of knocking down *meg* genes was verified by scoring the sterility of adult progeny of the worms exposed to RNAi.

To culture larger numbers of worms, worm cultures were started from synchronized L1s (hatched from embryos incubated in M9 overnight) onto NA22 or RNAi bacteria containing plates and grown to gravid adults at 20˚C. Early embryos were harvested from gravid adults.

To measure maternal-effect sterility of the *meg-1 meg-2(ax4532)* strain, 20 gravid adults from a mixed heterozygous population were singled out onto individual OP50 plates. Worms were allowed to lay eggs for 5 hours, then removed and genotyped by PCR. Adult progeny were scored for empty uteri (white sterile phenotype).

CRISPR genome editing

493 Genome editing was performed using CRISPR/Cas9 as described in Paix et al., 2017. The
494 *meg-1 meg-2* open reading frame was deleted with two guide RNAs targeting the following
495 sequences: 1. tgagcggcgatggataatcg and 2. agtcaaaattagttgctggg. Deletion of *meg-1 meg-2* was
496 confirmed by Sanger sequencing. This strain (JH3875) is maintained as a heterozygote because
497 the homozygous *meg-1 meg-2* deletion is 100% maternal effect sterile.
498
499 **RNA extraction and preparation of mRNA-seq library**
500 For each replicate, 26,000 synchronized L1 worms were plated on HT115 bacteria
501 transformed with either L4440 (control) or *meg-2* RNAi and grown at 20˚C until the young adult
502 stage. Adult worms were collected by filtering and the embryos were harvested by bleaching.
503 Embryo pellets were flash frozen in liquid nitrogen. RNA was extracted with TRIzol reagent and
504 chloroform. RNA was then concentrated and purified using Zymo's RNA Clean & Concentrator
505 kit.
506 For mRNA-seq library preparation, 1 µg of total RNA was treated with Ribo-Zero Gold
507 rRNA Removal Kit. A 1:100 dilution of ERCC RNA Spike-in Mix was added. Libraries were
508 prepared using the TruSeq stranded total RNA library Prep Kit with 12 cycles of PCR
509 amplification. All sequencing was performed using the Illumina HiSeq2500 at the Johns Hopkins
510 University School of Medicine Genetic Resources Core Facility.
511
512 **mRNA-sequencing analysis**
513 Sequencing reads were aligned to the UCSC ce10 *C. elegans* reference genome using
514 HISAT2 (Kim et al., 2015). Reads aligning to genetic features were then counted using HTSeq-
515 count (Anders et al., 2015) and analyzed for differential expression analysis using DESeq2 (Love
516 et al., 2014). Genes differentially expressed in wild-type vs *meg-1 meg-2* embryos are listed in
517 Table S3.
518
519 **Immunoprecipitation**
520 For each replicate for mass spec analysis, $1x10^6$ synchronized L1 worms were grown on
521 NA22 bacteria at 20˚C until the young adult stage. For IPs to compare MEG-1::GFP and MEG-

3::GFP by western blotting, 4x as many MEG-3::GFP embryos were collected as MEG-1::GFP embryos, because MEG-1 is ~4x more abundant than MEG-3 (Saha et al., 2016). Adult worms were collected by filtering and the embryos were harvested by bleaching. Embryos were washed and flash frozen in IP buffer (300 mM KCl, 50 mM HEPES pH 7.4, 1 mM EGTA, 1 mM $MgCl_2$, 1% glycerol, 0.1% NP-40) with 2x freshly prepared protease inhibitor mix #1 and mix #2 (100x protease inhibitor mix #1 contained 3 mg/mL antipain, 5 mg/mL leupeptin, 10 mg/mL benzamidine, 25 mg/mL AEBSF, and 1 mg/mL phosphoramidon diluted in PBS. 100x protease inhibitor mix #2 contained 5 mg/mL aprotinin, 4 mM bestatin, 1 mg/mL E64 and 1 mg/mL trypsin inhibitor diluted in water). Thawed embryos were sonicated on ice with a Branson Digital Sonifier SFX 250 with a microtip (15s on, 45s off, 15% power, 6 minutes total on time or until embryos were completely lysed) and cleared by centrifugation at 4˚C for 30 minutes at 20,817 RCF.

For the IP, 150 µl of anti-GFP nanobody conjugated to magnetic beads (Chromotek; cat# gtma-10) were incubated with the lysates at 4˚C for 90 minutes. The unbound fraction was removed and the beads were washed five times with ice cold IP buffer. The bound fraction was eluted by boiling the beads in 1% SDS with 50mM Tris-HCL pH 7.4 for 5 minutes.

Western blotting

1 M DTT and NuPAGE LDS sample buffer(4x) were added to lysates to a final concentration of 200 mM DTT and 1x NuPAGE LDS sample buffer. Samples were boiled for 5 minutes and run on 4-12% Bis-Tris gels in MES buffer. Samples were transferred to a PVDF membrane. Membranes were blocked in PBS with 0.1% Tween 20 and 5% non-fat dry milk (PBST + 5% milk). Membranes were incubated in primary antibodies diluted in PBST + 5% milk overnight at 4˚C. Membranes were washed three times for 10 minutes in PBST and then incubated with secondary antibodies diluted in PBST + 5% milk at room temperature for 1 hour. Membranes were washed again three times for 10 minutes in PBST and visualized with Pierce ECL Western Blotting Substrate (Thermo; cat# 32106) or SuperSignal West Femto Maximum Sensitivity Substrate (Thermo; cat# 34095) and the KwikQuantTM Imager (Kindle Biosciences).

Primary antibodies and concentrations used: mouse anti-GFP Living Colors (JL-8) (Takara Biosciences; cat# 632381) 1:500 dilution. Mouse anti-α-Tubulin (Sigma; cat# T6199) 1:1,000 dilution. Rabbit anti-POS-1 (a gift from Tom Evans) 1:500 dilution.

Mass spectrometry

Mass spectrometry was performed by the JHMI Mass Spectrometry and Proteomics Facility. Samples were reduced with DTT, alkylated with iodoacetamide, TCA/acetone precipitated, and in solution digested with trypsin. Samples were analyzed by LC-MS-MS on Q-Exactive Plus (Thermo) in FTFT at resolution 140K/35K with total 120 minute gradient.

Mass spec data analysis

Raw data were processed and analyzed using MaxQuant (2.0.3.0) software (Tyanova et al., 2016a). Default settings were used except that 'Match between runs' was turned on. Search parameters were as follows: Cysteine carbamidomethyl was included as a fixed modification, and variable modifications included oxidation of methionine, protein N-terminal acetylation, deamidation of glutamine and asparagine, and phosphorylation of serine, threonine and tyrosine, and the maximum number of modifications per peptide was set to 4. Trypsin was used as the digestion enzyme, a maximum of two missed cleavages were allowed, and the minimal peptide length was set to seven amino acids. Database search was performed against Uniprot *C. elegans* database (UP000001940_6239.fasta). False discovery rate (FDR) was set to 1% at peptide spectrum match (PSM) and protein level. Minimum peptide count required for protein quantification was set to two. Protein groups were further analyzed using Perseus (Tyanova et al., 2016b). Common contaminants, reverse proteins and proteins only identified by site were filtered out. LFQ values were $\log_2$ transformed. Two-sample *t-test*s were performed.

Immunostaining

Embryos were extruded from adult animals and subjected to freeze-crack on 0.01% poly-lysine coated slides followed by fixation in -20˚C methanol ≥ 15 minutes. Slides were blocked in PBS with 0.1% Tween 20 and 0.1% BSA (PBST + BSA) for 1 hour. Slides were

579 incubated in primary antibodies diluted in PBST + BSA at 4˚C in a humidity chamber overnight.
580 Slides were washed three times in PBST for 5 minutes and then incubated in secondary
581 antibodies diluted in PBST + BSA for 1 hour at room temperature. Slides were washed again
582 three times in PBST for 5 minutes, then two quick washes in PBS. Samples were mounted in
583 ProLong Glass Antifade mountant and cured overnight. When co-staining with OLLAS antibody,
584 the OLLAS primary and secondary were applied first to avoid cross reactions.
585 Primary antibodies and concentrations used: Mouse anti-FLAG M2 (Sigma; cat# F1804)
586 1:500. Rat anti-OLLAS L2 (Novus; cat# 06713) 1:50. Rabbit anti-CGH-1 (a gift from John Kim;
587 Alessi et al., 2015) 1:1,000. Rabbit anti-POS-1 (a gift from Tom Evans; Barbee and Evans, 2006)
588 1:100. Guinea pig anti-XND-1 (a gift from Judith Yanowitz; Wagner et al., 2010) 1:2,000. Mouse
589 anti-PGL-3 KT3 (DSHB) 1:100. Mouse anti-PGL-1 OIC1D4 (DSHB) 1:10. Mouse anti-UNC-54 mAB
590 5-8 (DSHB) 1:10. Anti-GFP nanobody conjugated to Alexa Fluor 488 (Chromotek; cat#
591 gb2AF488-10) 1:500. Antibody staining in this manuscript was consistent with that of previously
592 published works.
593
594 **Single molecule fluorescence in situ hybridization (smFISH)**
595 smFISH probes were designed using Biosearch Technologie's Stellaris Probe Designer.
596 Fluorophores used in this study were Quasar570 and Quasar670. For sample preparation,
597 embryos were extruded from adult animals and subjected to freeze-crack on 0.01% poly-lysine
598 coated slides followed by fixation in -20˚C methanol for ≥ 15 minutes. Slides were washed five
599 times in PBS with 0.1% Tween 20 (PBST) and fixed in 4% PFA in PBS for 1 hour at room
600 temperature. Slides were again washed four times in PBST, twice in 2x SSC, and once in wash
601 buffer (10% formamide, 2x SSC). Slides were then blocked in hybridization buffer (10%
602 formamide, 2x SSC, 200 µg/mL BSA, 2mM Ribonucleoside Vanadyl Complex, 0.2 mg/mL yeast
603 total RNA, 10% dextran sulfate) for 30 minutes at 37˚C in a humid chamber. For hybridization,
604 slides were incubated in 50-100 nM probe in hybridization buffer at 37˚C overnight. Slides were
605 then washed twice in wash buffer at 37˚C for 30 minutes, twice in 2x SSC, once in PBST and
606 twice in PBS. Samples were mounted in ProLong Glass Antifade mountant and cured overnight.
607

608 **Combined *in situ* hybridization/immunofluorescence**

609 Combined in situ hybridization with immunofluorescence was done by first doing the *in*
610 *situ* protocol as described above. After the last wash in PBS, the slides were then re-fixed in 4%
611 PFA for 1 hour at room temperature. The immunofluorescence protocol was then carried out as
612 described above except 1 mg/mL UltraPure BSA (Thermo, cat# AM2616) was used in the
613 blocking and antibody incubation steps. Primary antibody used: KT3 (DSHB) 1:100. Secondary
614 antibody used: goat anti-mouse IgA conjugated to FITC (abcam, cat# ab97234) 1:500.
615
616 **Laser scanning confocal microscopy**

617 Super-resolution microscopy was performed using a Zeiss LSM 880 microscope with a
618 63x-1.4 numerical aperture objective (Fig. 1, Fig. 3A, Fig. 4A, Fig. S1A,C, and Fig. S3A,B). The raw
619 data was processed using default Airyscan settings with ZEN software. For Fig. 4A,
620 representative high-resolution images were shown while the images used for quantification in
621 Fig. 4B were collected by spinning disk confocal microscopy. All images shown are single Z
622 slices.
623
624 **Spinning disk confocal microscopy**

625 All other microscopy was performed using a Zeiss Axio Observer equipped with a CSU-
626 W1 SoRA spinning disk scan head (Yokogawa). Images were taken using Slidebook software
627 software (Intelligent Imaging Innovations) with a 63x objective with a 2.8x relay lens
628 (Yokogawa). All images shown are single Z slices, except in Fig. 7C and D.
629
630 **Image quantification**

631 All images were quantified in Fiji. For profile plots to show colocalization of granule
632 components, a line was drawn through the center of a granule and the intensity along that line
633 was measured using the plot profile tool in Fiji. Since the size of each granule varied slightly, the
634 length of each plot was normalized to the smallest granule size. The intensities were then
635 binned using the averageifs function in Excel. The background signal was subtracted and the
636 intensities were normalized to the highest intensity.

637 For quantification of conditions that included sparse or asymmetrically localized
638 RNAs/Proteins in P_4, the sum intensity in P_4 above threshold was measured and normalized to
639 wild-type controls. The threshold was defined as being 1.5x the mean intensity of the entire
640 embryo. To minimize background, the smooth function in Fiji was used, which replaces each
641 pixel with the average of its 3x3 neighbors.
642 For quantification of symmetrically localized RNA/proteins in P_4, the ratio of the mean
643 intensity in the P blastomere over the mean intensity of a same sized region in the soma was
644 measured. A background measurement was taken from outside the embryo and subtracted
645 from the germline and soma intensities. The ratios were then normalized to wild type.
646 To assess the segregation of PGL-3 (Fig. S1D), DDX6^{CGH-1} and EDC-3 (Fig. S4) into P
647 blastomeres, the mean intensity was measured in each P blastomere and were then normalized
648 to the average P_0 intensity.
649 To measure the ratio of RNA inside/outside of granules, the granule (labeled by MEG-
650 1::GFP in Fig. 3B, SL1 in Fig. S5 or PGL-3 in Fig. S7) was defined as being 1.5x above the mean
651 intensity of the signal within the P blastomere. The mean intensity inside and outside the
652 granule in the cytoplasm was measured. A background signal was taken from a region outside
653 the embryo and subtracted.
654
655 **Statistical analysis and plotting**
656 Perseus (Tyanova et al., 2016b) was used for *t*-tests on mass spec data. To determine
657 the significance of the enrichment of P-body proteins in MEG-1 immunoprecipitates, we
658 assumed a total pool of 6,000 proteins, which is roughly the size of the embryonic proteome
659 (Saha et al., 2016).
660 Statistics for differential expression analysis were done using DESeq2 (Love et al., 2014).
661 To determine the significance of the overlap between predicted POS-1 targets (Elewa et al.,
662 2015) and *meg-1 meg-2* differentially expressed genes, we assumed a total pool of 11,121
663 transcripts. We arrived at this number by setting an FPKM threshold in our RNA-seq analysis of
664 0.002178852 FPKM, which was the lowest FPKM in *meg-1 meg-2* animals that we were able to

665 detect a significant increase in gene expression. Any non-protein coding genes were also
666 identified and removed from the list by using the SimpleMine tool on WormBase.
667 All other statistical analysis was conducted using R or Graphpad Prism 9 software. Data
668 were plotted with either Graphpad Prism 9 or ggplot2 (Wickham, 2016).
669
670 **References**
671
672 Alessi, A. F., Khivansara, V., Han, T., Freeberg, M. A., Moresco, J. J., Tu, P. G., … Kim, J. K. (2015).
673 Casein kinase II promotes target silencing by miRISC through direct phosphorylation of the
674 DEAD-box RNA helicase CGH-1. *Proceedings of the National Academy of Sciences of the United*
675 *States of America* 112, E7213–E7222.
676
677 Anders, S., Pyl, P.T., and Huber, W. (2015). HTSeq–a Python framework to work with high-
678 throughput sequencing data. *Bioinformatics* 31, 166–169.
679
680 Aravin, A. A., Van Der Heijden, G. W., Castaneda, J., Vagin, V. V., Hannon, G. J., and Bortvin, A.
681 (2009). Cytoplasmic compartmentalization of the fetal piRNA pathway in mice. *PLoS Genetics* 5,
682 e1000764.
683
684 Arkov, A. L., and Ramos, A. (2010). Building RNA-protein granules: Insight from the germline.
685 *Trends in Cell Biology* 20, 482–490.
686
687 Barbee, S. A. and Evans, T. C. (2006). The Sm proteins regulate germ cell specification during
688 early *C. elegans* embryogenesis. *Developmental Biology* 291, 132–143.
689
690 Boag, P. R., Atalay, A., Robida, S., Reinke, V., and Blackwell, T. K. (2008). Protection of specific
691 maternal messenger RNAs by the P-body protein CGH-1 (Dhh1/RCK) during *Caenorhabditis*
692 *elegans* oogenesis. *Journal of Cell Biology* 182, 543–557.
693

694 Boag, P. R., Nakamura, A., and Blackwell, T. K. (2005). A conserved RNA-protein complex
695 component involved in physiological germline apoptosis regulation in *C. elegans*. *Development*
696 132, 4975–4986.
697
698 Brangwynne, C.P., Eckmann, C.R., Courson, D.S. Rybarska, A., Hoege, C., Gharakhani, J., Jülicher,
699 F., and Hyman, A.A. (2009). Germline P granules are liquid droplets that localize by controlled
700 dissolution/condensation. *Science* 324, 1729–1732.
701
702 Brenner, S. (1974). The genetics of *Caenorhabditis elegans*. *Genetics* 77, 71-94.
703
704 Cao, W. X., Kabelitz, S., Gupta, M., Yeung, E., Lin, S., Rammelt, C., … Lipshitz, H. D. (2020).
705 Precise Temporal Regulation of Post-transcriptional Repressors Is Required for an Orderly
706 Drosophila Maternal-to-Zygotic Transition. *Cell Reports* 31, 107783.
707
708 Ciais, D., Cherradi, N., and Feige, J. J. (2013). Multiple functions of tristetraprolin/TIS11 RNA-
709 binding proteins in the regulation of mRNA biogenesis and degradation. *Cellular and Molecular*
710 *Life Sciences* 70, 2031–2044.
711
712 D'Agostino, I., Merritt, C., Chen, P. L., Seydoux, G., and Subramaniam, K. (2006). Translational
713 repression restricts expression of the *C. elegans* Nanos homolog NOS-2 to the embryonic
714 germline. *Developmental Biology* 292, 244–252.
715
716 DeMott, E., Dickinson, D.J., Doonan, R. (2021). Highly improved cloning efficiency for plasmid-
717 based CRISPR knock-in in *C. elegans*. *microPublication Biology*
718 10.17912/micropub.biology.000499.
719
720 Di Stefano, B., Luo, E. C., Haggerty, C., Aigner, S., Charlton, J., Brumbaugh, J., … Hochedlinger, K.
721 (2019). The RNA Helicase DDX6 Controls Cellular Plasticity by Modulating P-Body
722 Homeostasis. *Cell Stem Cell* 25, 622-638.

Dodson, A. E., and Kennedy, S. (2019). Germ Granules Coordinate RNA-Based Epigenetic Inheritance Pathways. *Developmental Cell* 50, 704-715.

Eckmann, C. R., Kraemer, B., Wickens, M., and Kimble, J. (2002). GLD-3, a bicaudal-C homolog that inhibits FBF to control germline sex determination in *C. elegans*. *Developmental Cell* 3, 697–710.

Eichler, C. E., Hakes, A. C., Hull, B., and Gavis, E. R. (2020). Compartmentalized *oskar* degradation in the germ plasm safeguards germline development. *ELife* 9, e49988.

Elewa, A., Shirayama, M., Kaymak, E., Harrison, P. F., Powell, D. R., Du, Z., … Mello, C. C. (2015). POS-1 Promotes Endo-mesoderm Development by Inhibiting the Cytoplasmic Polyadenylation of *neg-1* mRNA. *Developmental Cell* 34, 108–118.

Farley, B. M., Pagano, J. M., and Ryder, S. P. (2008). RNA target specificity of the embryonic cell fate determinant POS-1. *RNA* 14, 2685–2697.

Folkmann, A. W., Putnam, A., Lee, C. F., and Seydoux, G. (2021). Regulation of biomolecular condensates by interfacial protein clusters. *Science* 373, 1218–1224.

Francis, R., Barton, M.K., Kimble, J., and Schedl, T. (1995). *gld-1*, a tumor suppressor gene required for oocyte development in *Caenorhabditis elegans*. *Genetics* 139, 579–606.

Gallo, C. M., Munro, E., Rasoloson, D., Merritt, C., and Seydoux, G. (2008). Processing bodies and germ granules are distinct RNA granules that interact in *C. elegans* embryos. *Developmental Biology* 323, 76–87.

751 Gallo, C. M., Wang, J. T., Fumio, M., and Seydoux, G. (2010). Cytoplasmic Partitioning of P
752 Granule Components Is Not Required to Specify the Germline in *C. elegans*. *Science* 330, 1685–
753 1689.
754
755 Han, B., Antkowiak, K. R., Fan, X., Rutigliano, M., Ryder, S. P., and Griffin, E. E. (2018). Polo-like
756 Kinase Couples Cytoplasmic Protein Gradients in the C. elegans Zygote. *Current Biology* 28, 60-
757 69.
758
759 Hanazawa, M., Yonetani, M., and Sugimoto, A. (2011) PGL proteins self associate and bind RNPs
760 to mediate germ granule assembly in *C. elegans*. *Journal of Cell Biology* 192, 929–937.
761
762 Hubatsch, L., Peglion, F., Reich, J. D., Rodrigues, N. T. L., Hirani, N., Illukkumbura, R., and
763 Goehring, N. W. (2019). A cell-size threshold limits cell polarity and asymmetric division
764 potential. *Nature Physics* 15, 1078–1085.
765
766 Ivanov, P., Kedersha, N., and Anderson, P. (2019). Stress granules and processing bodies in
767 translational control. *Cold Spring Harbor Perspectives in Biology* 11, a032813.
768
769 Jadhav, S., Rana, M., and Subramaniam, K. (2008). Multiple maternal proteins coordinate to
770 restrict the translation of *C. elegans nanos-2* to primordial germ cells. *Development* 135, 1803–
771 1812.
772
773 Jensen, L., Venkei, Z. G., Watase, G. J., Bisai, B., Pletcher, S., Lee, C. Y., and Yamashita, Y. M.
774 (2021). *me31B* regulates stem cell homeostasis by preventing excess dedifferentiation in the
775 *Drosophila* male germline. *Journal of Cell Science* 134, 1-10.
776
777 Jones, A.R., Francis, R., and Schedl, T. (1996). GLD-1, a cytoplasmic protein essential for oocyte
778 differentiation, shows stage- and sex-specific expression during Caenorhabditis elegans
779 germline development. *Developmental Biology* 180, 165–183.

780

781 Kapelle, W. S., and Reinke, V. (2011). *C. elegans meg-1* and *meg-2* differentially interact with
782 *nanos* family members to either promote or inhibit germ cell proliferation and
783 survival. *Genesis* 49, 380–391.
784
785 Kemph, A. and Lynch, J. A. (2022). Evolution of germ plasm assembly and function among the
786 insects. *Current Opinion in Insect Science* 50, 100883.
787
788 Kim, D., Langmead, B., and Salzberg, S.L. (2015). HISAT: a fast spliced aligner with low memory
789 requirements. *Nat. Methods* 12, 357–360.
790
791 Kipreos, E. T. (2005). Ubiquitin-mediated pathways in *C. elegans*. *WormBook: The Online Review*
792 *of C. Elegans Biology*, 1–24.
793
794 Kulkarni, A. and Extavour, C. G. (2017). Convergent evolution of germ granule nucleators: A
795 hypothesis. *Stem Cell Research* 24, 188–194.
796
797 Leacock, S.W. and Reinke, V. (2008). MEG-1 and MEG-2 are embryo-specific P-granule
798 components required for germline development in *Caenorhabditis elegans*. *Genetics* 178, 295–
799 306.
800
801 Lee, C.Y. S., Lu, T., and Seydoux, G. (2017). Nanos promotes epigenetic reprogramming of the
802 germline by down-regulation of the THAP transcription factor LIN-15B. *ELife* 6, e30201.
803
804 Lee, C. Y. S., Putnam, A., Lu, T., He, S., Ouyang, J. P. T., and Seydoux, G. (2020). Recruitment of
805 mRNAs to P granules by condensation with intrinsically-disordered proteins. *ELife* 9, e52896.
806
807 Love, M. I., Huber, W., and Anders, S. (2014). Moderated estimation of fold change and
808 dispersion for RNA-seq data with DESeq2. *Genome Biology* 15, 550.

Mainpal, R., Nance, J., and Yanowitz, J. L. (2015). A germ cell determinant reveals parallel pathways for germ line development in *Caenorhabditis elegans*. *Development* 142, 3571–3582.

McCambridge, A., Solanki, D., Olchawa, N., Govani, N., Trinidad, J. C., and Gao, M. (2020). Comparative Proteomics Reveal Me31B's Interactome Dynamics, Expression Regulation, and Assembly Mechanism into Germ Granules during *Drosophila* Germline Development. *Scientific Reports* 10, 1–13.

Neil, C. R., Jeschonek, S. P., Cabral, S. E., O'Connell, L. C., Powrie, E. A., Otis, J. P., … Mowry, K. L. (2021). L-bodies are RNA-protein condensates driving RNA localization in Xenopus oocytes. *Molecular Biology of the Cell* 32, ar37.

Nicklas, S., Okawa, S., Hillje, A. L., González-Cano, L., Sol, A. D., and Schwamborn, J. C. (2015). The RNA helicase DDX6 regulates cell-fate specification in neural stem cells via miRNAs. *Nucleic Acids Research* 43, 2638–2654.

Noble, S. L., Allen, B. L., Goh, L. K., Nordick, K., and Evans, T. C. (2008). Maternal mRNAs are regulated by diverse P-body-related mRNP granules during early *Caenorhabditis elegans* development. *Journal of Cell Biology* 182, 559–572.

Ouyang, J. P. T., Folkmann, A., Bernard, L., Lee, C. Y., Seroussi, U., Charlesworth, A. G., … Seydoux, G. (2019). P Granules Protect RNA Interference Genes from Silencing by piRNAs. *Developmental Cell* 50, 716-728.

Paix, A., Folkmann, A., and Seydoux, G. (2017). Precision genome editing using CRISPR-Cas9 and linear repair templates in *C. elegans*. *Methods* 121-122, 86–93.

Paix, A., Wang, Y., Smith, H. E., Lee, C. Y. S., Calidas, D., Lu, T., … Seydoux, G. (2014). Scalable and versatile genome editing using linear DNAs with microhomology to Cas9 sites in *Caenorhabditis elegans*. *Genetics* 198, 1347–1356.

Phillips, C. M. and Updike, D. L. (2022). Germ granules and gene regulation in the *Caenorhabditis elegans* germline. *Genetics* 220, iyab195.

Putnam, A., Cassani, M., Smith, J., and Seydoux, G. (2019). A gel phase promotes condensation of liquid P granules in *Caenorhabditis elegans* embryos. *Nature Structural and Molecular Biology* 26, 220–226.

Roovers, E. F., Kaaij, L. J. T., Redl, S., Bronkhorst, A. W., Wiebrands, K., de Jesus Domingues, A. M., … Ketting, R. F. (2018). Tdrd6a Regulates the Aggregation of Buc into Functional Subcellular Compartments that Drive Germ Cell Specification. *Developmental Cell* 46, 285-301.

Saha, S., Weber, C. A., Nousch, M., Adame-Arana, O., Hoege, C., Hein, M. Y., … Hyman, A. A. (2016). Polar Positioning of Phase-Separated Liquid Compartments in Cells Regulated by an mRNA Competition Mechanism. *Cell* 166, 1572-1584.

Scheckel, C., Gaidatzis, D., Wright, J. E., and Ciosk, R. (2012). Genome-wide analysis of GLD-1-mediated mRNA regulation suggests a role in mRNA storage. *PLoS Genetics* 8, 1–12.

Schmidt, H., Putnam, A., Rasoloson, D., and Seydoux, G. (2021). Protein-based condensation mechanisms drive the assembly of RNA-rich P granules. *ELife* 10, e63698.

Seydoux, G., and Fire, A. (1994). Soma-germline asymmetry in the distributions of embryonic RNAs in Caenorhabditis elegans. *Development* 120, 2823–2834.

865 Shimada, R., Kiso, M., and Saga, Y. (2019). ES-mediated chimera analysis revealed requirement
866 of DDX6 for NANOS2 localization and function in mouse germ cells. *Scientific Reports* 9, 1-12.
867
868 Smith, J., Calidas, D., Schmidt, H., Lu, T., Rasoloson, D., and Seydoux, G. (2016). Spatial
869 patterning of P granules by RNA-induced phase separation of the intrinsically-disordered
870 protein MEG-3. *ELife* 5, e21337.
871
872 Strome, S., Martin, P., Schierenberg, E., and Paulsen, J. (1995). Transformation of the germ line
873 into muscle in *mes-1* mutant embryos of *C. elegans*. *Development* 121, 2961–2972.
874
875 Strome, S. and Wood, W. B. (1982). Immunofluorescence visualization of germ-line-specific
876 cytoplasmic granules in embryos, larvae, and adults of *Caenorhabditis elegans*. *Proceedings of*
877 *the National Academy of Sciences of the United States of America* 79, 1558–1562.
878
879 Subramaniam, K. and Seydoux, G. (1999). *nos-1* and *nos-2*, two genes related to *Drosophila*
880 *nanos*, regulate primordial germ cell development and survival in *Caenorhabditis elegans*.
881 *Development* 126, 4861–4871.
882
883 Suzuki, A., Igarashi, K., Aisaki, K. I., Kanno, J., and Saga, Y. (2010). NANOS2 interacts with the
884 CCR4-NOT deadenylation complex and leads to suppression of specific RNAs. *Proceedings of the*
885 *National Academy of Sciences of the United States of America* 107, 3594–3599.
886
887 Tabara, H., Hill, R. J., Mello, C. C., Priess, J. R., and Kohara, Y. (1999). *pos-1* encodes a
888 cytoplasmic zinc-finger protein essential for germline specification in *C.*
889 *elegans*. *Development* 126, 1–11.
890
891 Timmons, L. and Fire, A. (1998). Specific interference by ingested dsRNA. *Nature* 395, 854.
892

Tintori, S. C., Osborne Nishimura, E., Golden, P., Lieb, J. D., and Goldstein, B. (2016). A Transcriptional Lineage of the Early *C. elegans* Embryo. *Developmental Cell* 38, 430–444.

Tyanova, S., Temu, T., and Cox, J. (2016a) The MaxQuant computational platform for mass spectrometry-based shotgun proteomics. *Nature Protocols* 11, 2301–2319.

Tyanova, S., Temu, T., Sinitcyn, P., Carlson, A., Hein, M.Y., Geiger, T., Mann, M., and Cox, J. (2016b) The Perseus computational platform for comprehensive analysis of (prote)omics data *Nature Methods* 13, 731–740.

Uebel, C. J., Agbede, D., Wallis, D. C., and Phillips, C. M. (2020). Mutator foci are regulated by developmental stage, RNA, and the germline cell cycle in *Caenorhabditis elegans*. *G3: Genes, Genomes, Genetics* 10, 3719–3728.

Uebel, C. J., Manage, K. I., and Phillips, C. M. (2021). SIMR foci are found in the progenitor germ cells of *C. elegans* embryos. *MicroPublication Biology* 10.17912/micropub.biology.000374.

Updike, D. L., Hachey, S. J., Kreher, J., and Strome, S. (2011). P granules extend the nuclear pore complex environment in the *C. elegans* germ line. *Journal of Cell Biology* 192, 939–948.

Vo, H. D. L., Wahiduzzaman, Tindell, S. J., Zheng, J., Gao, M., and Arkov, A. L. (2019). Protein components of ribonucleoprotein granules from Drosophila germ cells oligomerize and show distinct spatial organization during germline development. *Scientific Reports* 9, 1–12.

Wagner, C. R., Kuervers, L., Baillie, D. L., and Yanowitz, J. L. (2010). *xnd-1* regulates the global recombination landscape in *Caenorhabditis elegans*. *Nature* 467, 839–843.

Wan, G., Fields, B. D., Spracklin, G., Shukla, A., Phillips, C. M., and Kennedy, S. (2018). Spatiotemporal regulation of liquid-like condensates in epigenetic inheritance. *Nature* 557, 679–683.

Wang, J.T., Seydoux, G. (2013). Germ Cell Specification. In: Schedl, T. (eds) Germ Cell Development in *C. elegans*. Advances in Experimental Medicine and Biology, vol 757. Springer, New York, NY.

Wang, J.T., Smith, J., Chen, B. C., Schmidt, H., Rasoloson, D., Paix, A., … Seydoux, G. (2014). Regulation of RNA granule dynamics by phosphorylation of serine-rich, intrinsically disordered proteins in *C. elegans*. *ELife* 3, e04591.

Wang, L., Eckmann, C. R., Kadyk, L. C., Wickens, M., and Kimble, J. (2002). A regulatory cytoplasmic poly(A) polymerase in *Caenorhabditis elegans*. *Nature* 419, 312–316.

Wickham, H. (2016). *ggplot2: Elegant Graphics for Data Analysis*. New York: Springer-Verlag.

Wright, D., Kiso, M., and Saga, Y. (2021). Genetic and structural analysis of the in vivo functional redundancy between murine NANOS2 and NANOS3. *Development* 148, 1–12.

Wu, E., Vashisht, A. A., Chapat, C., Flamand, M. N., Cohen, E., Sarov, M., … Duchaine, T. F. (2017). A continuum of mRNP complexes in embryonic microRNA-mediated silencing. *Nucleic Acids Research* 45, 2081–2098.

Yang, C., Dominique, G. M., Champion, M. M., and Huber, P. W. (2022). Remnants of the Balbiani body are required for formation of RNA transport granules in *Xenopus* oocytes. *IScience* 25, 103878.

948 Zavortink, M., Rutt, L. N., Dzitoyeva, S., Henriksen, J. C., Barrington, C., Bilodeau, D. Y., …
949 Rissland, O. S. (2020). The E2 Marie Kondo and the CTLH E3 ligase clear deposited RNA binding
950 proteins during the maternal-to-zygotic transition. *ELife* 9, e53889.

951

952

953

954 **Supplemental table 1: Sterility of *meg-1 meg-2(ax4532)* mutant.**

Genotype	**percent sterile (n)**
MEG-1::GFP/*meg-1 meg-2 (ax4532)* (+/-)	0 (289)
meg-1 meg-2 (ax4532)/meg-1 meg-2 (ax4532) (-/-)	100 (156)

955

956

957 **Supplemental table 4: Strains used.**

Designation	**Genotype**	**Citation**
JH1	N2	Brenner, 1974
JH2878	*meg-1(vr10)* X	Leacock and Reinke, 2008
JH3475	*meg-3(ax3055) meg-4(ax3052)* X	Smith et al., 2016
JH3229	*meg-1(vr10) meg-3(tm4259)* X	Wang et al., 2014
JH3875	*meg-1 meg-2(ax4532)/meg-1(ax4534[meg-1::gfp])* X	this study
JH3888	*meg-3(ax3051[meg-3::OLLAS]) meg-4(ax2080[meg-4::3xFLAG]) meg-1 meg-2(ax4532)/meg-1(ax4534[meg-1::gfp])* X	this study
JH3379	*meg-1(ax4534[meg-1::gfp])* X	this study
JH3472	*meg-1(ax4534[meg-1::gfp]) meg-3(tm4259) meg-4(ax2026)* X	this study
JH4181	*meg-1(ax4534[meg-1::gfp]) meg-3(ax3051[meg-3::OLLAS]) meg-4(ax2080[meg-4::3xFLAG])* X	this study

JH3852	*pgl-3(ax4300[pgl-3::mCherry])* V; *meg-1(ax4534[meg-1::gfp])* X	this study
JH3503	*meg-3(ax3054[meg-3::meGFP])* X	Smith et al., 2016
JH4219	*meg-3(ax3054[meg-3::meGFP]) meg-1(vr10)* X	this study
GLW43	*edc-3(utx35[mNG::3xFlag::edc-3])* I	DeMott et al., 2021
JH4176	*edc-3(utx35[mNG::3xFlag::edc-3])* I; *meg-1(vr10)* X	this study
JH4177	*edc-3(utx35[mNG::3xFlag::edc-3])* I; *meg-3(ax3055) meg-4(ax3052)* X	this study
JH4178	*edc-3(utx35[mNG::3xFlag::edc-3])* I; *meg-1(vr10) meg-3(tm4259)* X	this study
JH4180	*edc-3(utx35[mNG::3xFlag::edc-3])* I; *meg-1(ax4535[meg-1::ollas]) meg-3(ax3055) meg-4(ax3052)* X	this study
JH3193	*nos-2(ax2049[3xflag::nos-2])* II	Paix et al., 2014
JH3410	*nos-2(ax2049[3xflag::nos-2])* II; *meg-1(vr10)* X	this study
JH4258	*nos-2(ax2049[3xflag::nos-2])* II; *meg-3(ax3055) meg-4(ax3052)* X	Lee et al., 2020
JH3882	*nos-2(ax2049[3xflag::nos-2])* II; *meg-1(vr10) meg-3(tm4259)* X	this study
JH3605	*Y51F10.2(ax4319[Y51F10.2::OLLAS])* I	Lee et al., 2020
JH3880	*Y51F10.2(ax4319[Y51F10.2::OLLAS])* I; *meg-1(vr10)* X	this study
JH3611	*Y51F10.2(ax4319[Y51F10.2::OLLAS])* I; *meg-3(ax3055) meg-4(ax3052)* X	Lee et al., 2020
JH3881	*Y51F10.2(ax4319[Y51F10.2::OLLAS])* I; *meg-1(vr10) meg-3(tm4259)* X	this study
JH3207	*deps-1(ax2063[deps-1::GFP])* I	Paix et al., 2014
JH3404	*deps-1(ax2063[deps-1::GFP])* I; *meg-1(vr10)*	this study

JH3352	*deps-1(ax2063[deps-1::GFP])* I; *meg-3(tm4259) meg-4(ax2026)* X	this study
YY1325	*wago-4(gg620[3xflag::gfp::wago-4])* II	Wan et al., 2018
JH3871	*wago-4(gg620[3xflag::gfp::wago-4])* II; *meg-1(vr10)* X	this study

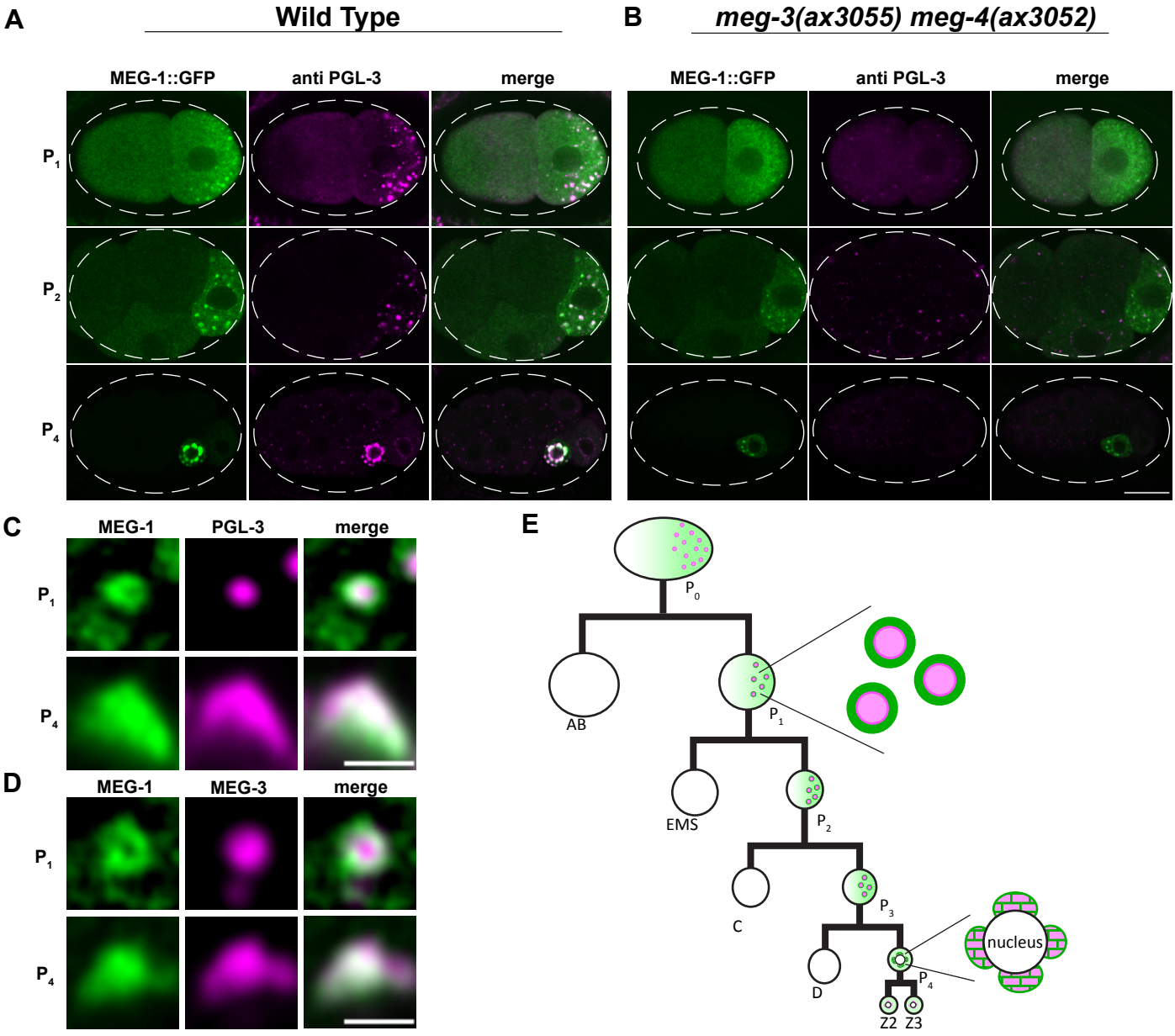

Fig. 1: MEG-1 puncta are distinct from P granules.

Representative Airyscan photomicrographs of wild-type (A) and *meg-3 meg-4* mutant (B) embryos expressing endogenous MEG-1::GFP and co-stained for GFP and PGL-3. MEG-1, but not PGL-3, enriches in P blastomeres in *meg-3 meg-4* embryos. Scale bar is 10 μm. (C and D) Higher resolution images of MEG-1::GFP and PGL-3 (C) and MEG-1::GFP and MEG-3::OLLAS (D) in P_1 and P_4. In P_1, MEG-1 enriches at the periphery of PGL-3 and MEG-3. In P_4, P granules become perinuclear and MEG-1 and PGL-3/MEG-3 overlap. See Fig. S1A for quantification. Scale bars are 1 μm. (E) Abbreviated cartoon lineage summarizing the distribution of MEG-1 (green) and P granules (pink) in the germline (P) blastomeres. In the zygote P_0, MEG-1 is present in a cytoplasmic gradient as well as small granules that are difficult to visualize at this stage. MEG-1 enriches at the periphery of P granules in the P_{1-3} blastomeres, and merges with P granules in P_4. In the primordial germ cells Z2 and Z3, MEG-1 becomes cytoplasmic and is degraded, while P granules remain.

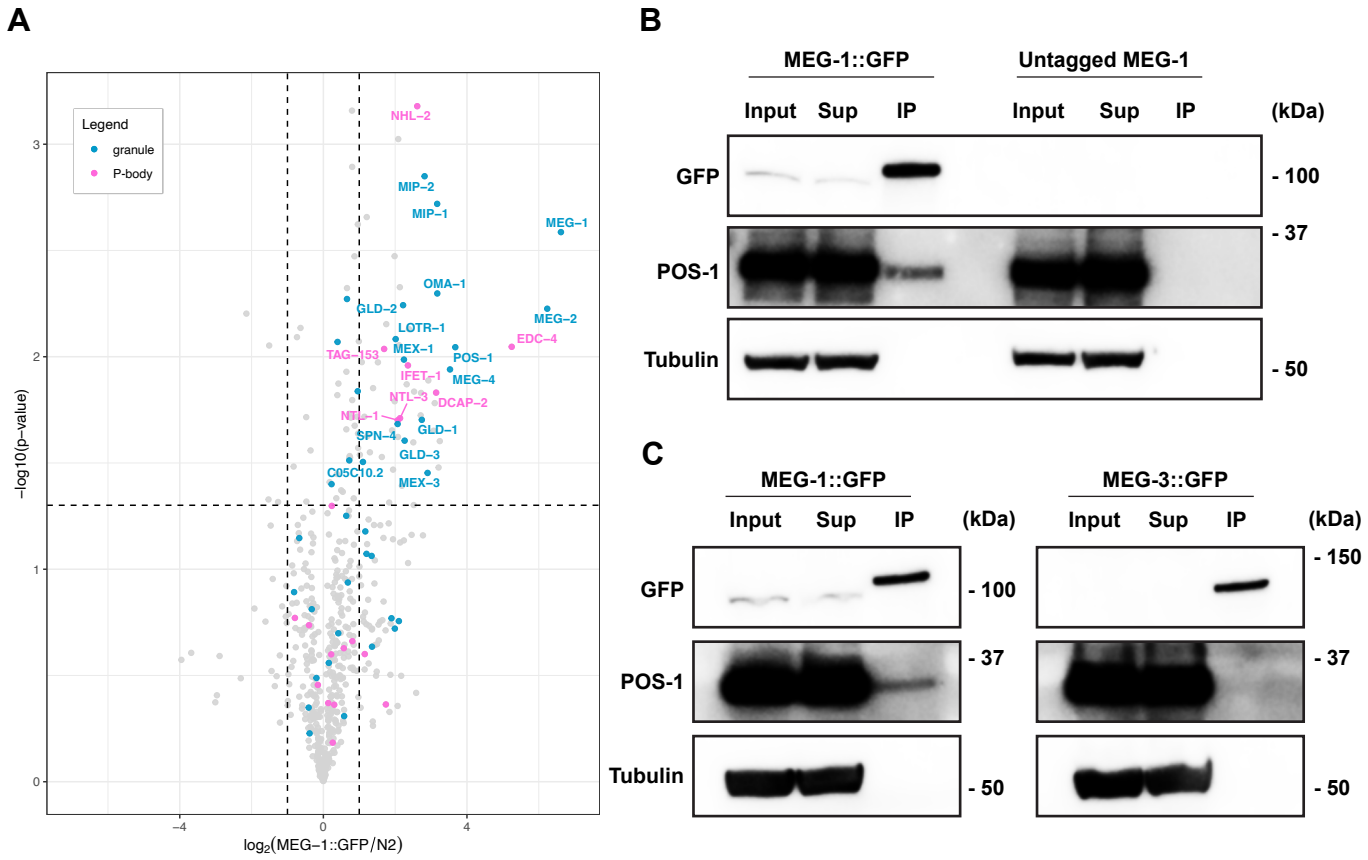

Fig. 2: MEG-1 immunoprecipitates with P-body and RNA-binding proteins, including POS-1.

(A) Volcano plot showing on the X-axis the log2 fold enrichment of proteins (dots) in MEG-1::GFP immunoprecipitates over "N2" (wild-type lysates containing untagged MEG-1) as a function of the log10 *p*-value calculated from two independent immunoprecipitation experiments (Y-axis). Of the 54 proteins enriched in MEG-1::GFP immunoprecipitates (top right quadrant), 13% correspond to P-body proteins (labeled in pink) and 28% correspond to proteins previously reported to localize to granules in P blastomeres (blue). (B) Representative western blots from two independent experiments confirm that GFP immunoprecipitates pull down MEG-1::GFP and POS-1, but not tubulin. (C) Western blots from MEG-1::GFP and MEG-3::GFP immunoprecipitates. Unlike MEG-1::GFP, MEG-3::GFP does not pull down POS-1. Full western blot images are shown in Fig. S2.

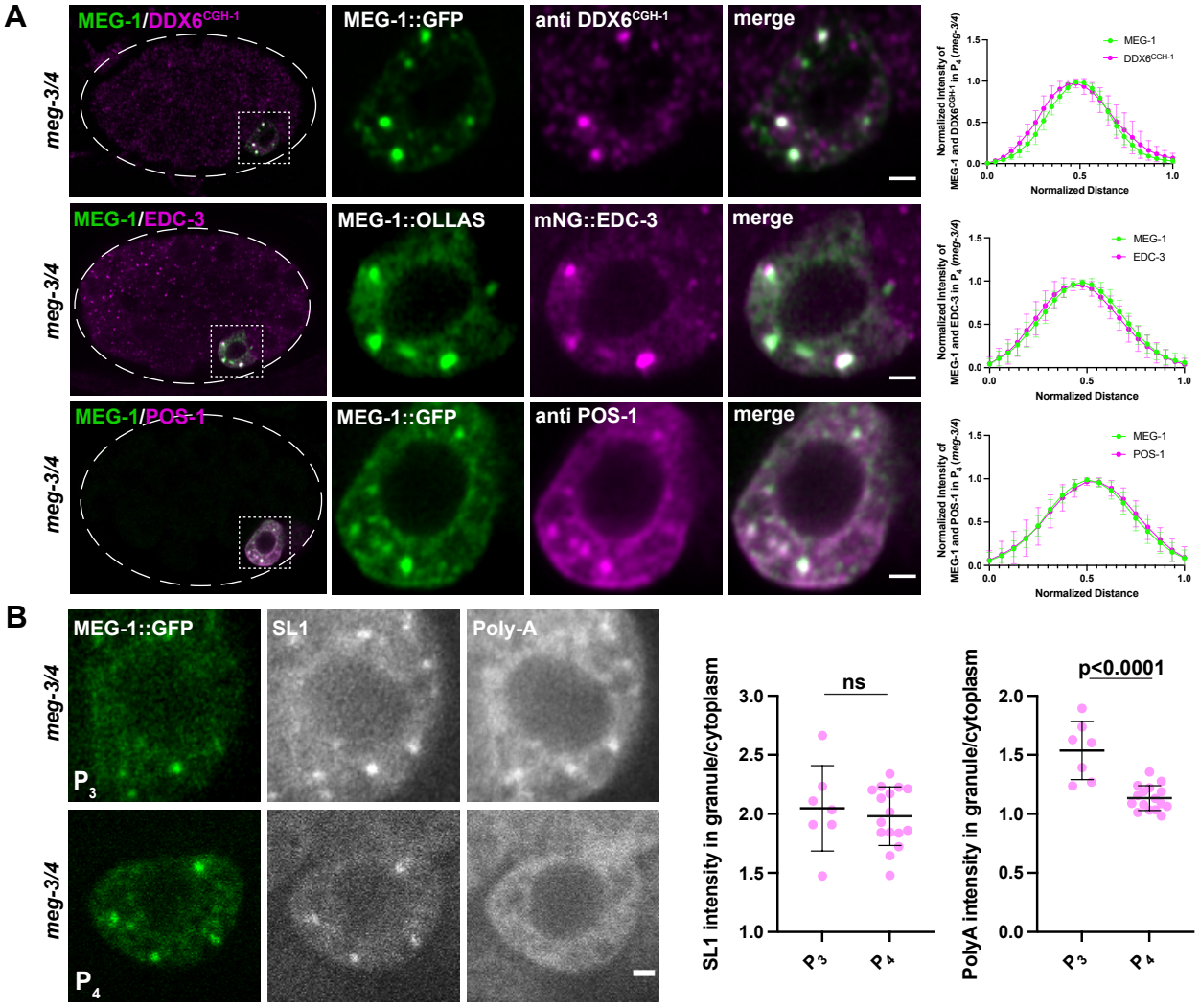

Fig. 3: MEG-1 puncta in P_4 correspond to germline P-bodies.

(A) Airyscan photomicrographs of *meg-3 meg-4* embryos expressing MEG-1::GFP and co-stained for GFP and DDX6^{CGH-1}, expressing MEG-1::OLLAS and mNG::3xFLAG::EDC-3 and co-stained for OLLAS and FLAG, and expressing MEG-1::GFP and co-stained for GFP and POS-1. Inset shows P_4 blastomere. Graphs plotting the mean intensities through the center of a granule indicate colocalization. For MEG-1 and DDX6^{CGH-1} n= 7 granules from 2 embryos, for MEG-1 and EDC-3 n=9 granules from 2 embryos, for MEG-1 and POS-1 n=10 granules from 2 embryos. (B) Photomicrographs of *meg-3 meg-4* embryos expressing MEG-1::GFP and probed for SL1 and poly-A. MEG-1 foci enrich SL1 to similar levels in P_3 and P_4, but show higher enrichment of poly-A in P_3 compared to P_4. The ratio of SL1 or poly-A intensity in MEG-1 granules over cytoplasm in P_3 (n=7) was compared to P_4 (n=16). Significance calculated by *t*-test. Quantification for each genotype is from one experiment where several mutant and control animals were processed in parallel. All error bars represent mean ± s.d. All scale bars are 1 μm.

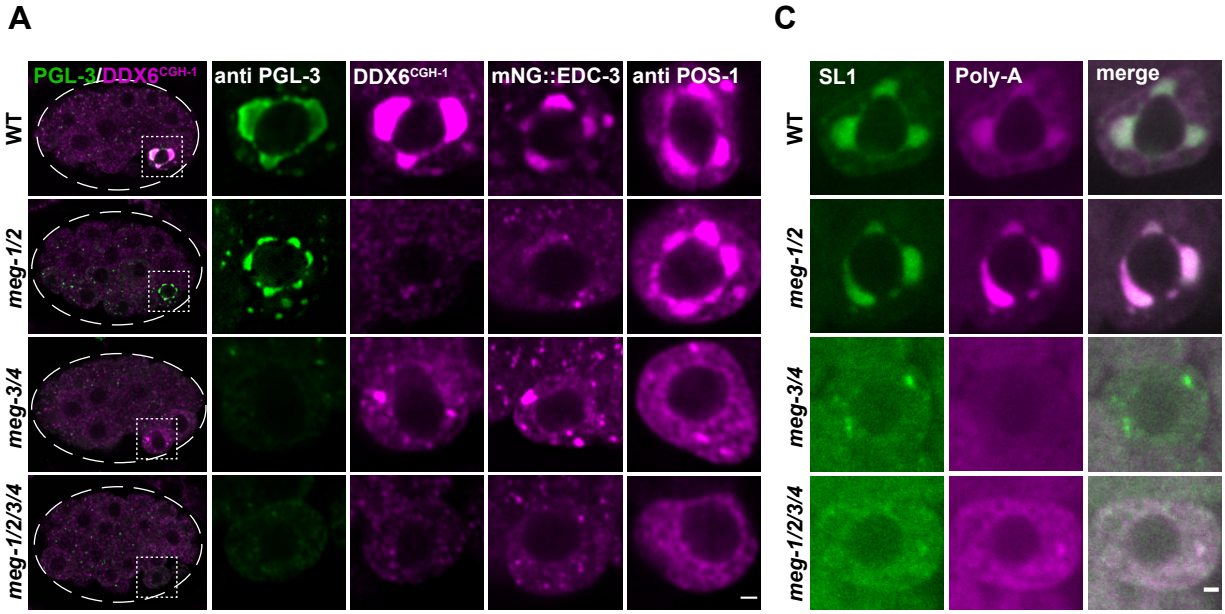

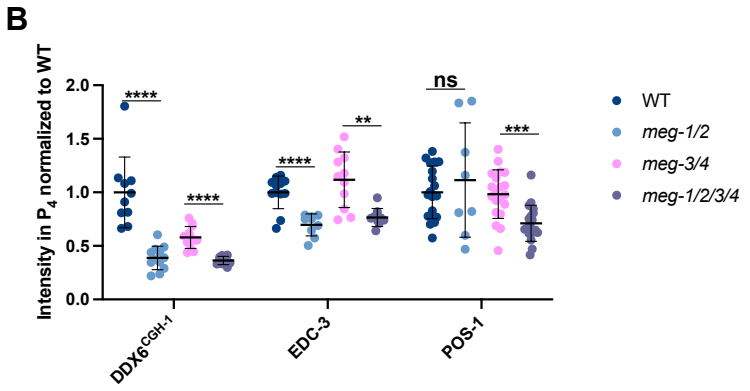

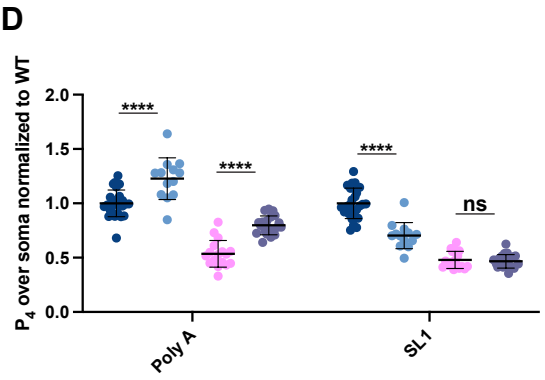

Fig. 4: MEG-1/2 are required for maintenance of germline P-bodies in P_4.
(A) Airyscan photomicrographs of embryos of the indicated *meg* genotypes co-stained for PGL-3 and $DDX6^{CGH-1}$ (whole embryo and P_4 inset), or expressing mNG::3xFLAG::EDC-3 and stained for FLAG, or stained for POS-1. *meg-1 meg-2* are not essential for localization of PGL-3 or POS-1 to P_4 but are required for maintenance of $DDX6^{CGH-1}$ and EDC-3. (B) Intensity of $DDX6^{CGH-1}$, EDC-3 and POS-1 in P_4 relative to wild type. Quantification of $DDX6^{CGH-1}$ for each genotype is from one experiment where mutant and control animals were processed in parallel. Wild type n=10; *meg-1/2* n=12; *meg-3/4* n=12; *meg-1/2/3/4* n=10. Quantification of EDC-3 for each genotype is from one experiment where mutant and control animals were processed in parallel. Wild type n=12; *meg-1/2* n=9; *meg-3/4* n=11; *meg-1/2/3/4* n=9. Quantification of POS-1 for *meg-1 meg-2* embryos is from one experiment and from *meg-3 meg-4* and *meg-1 meg-2 meg-3 meg-4* are from two experiments where mutant and control animals were processed in parallel. Wild type n=19; *meg-1/2* n=8; *meg-3/4* n=20; *meg-1/2/3/4* n=19. (C) Photomicrographs of P_4 in the indicated genotypes probed for SL1 and poly-A. Poly-A levels are increased in *meg-1 meg-2* mutants, despite SL1 levels decreasing or not changing. (D) Quantification of poly-A and SL1 in P_4 over soma normalized to wild type. Quantification for *meg-1 meg-2* embryos are from two experiments and from *meg-3 meg-4* and *meg-1 meg-2 meg-3 meg-4* are from three experiments where mutant and control animals were processed in parallel. Wild type n=26; *meg-1/2* n=13; *meg-3/4* n=17; *meg-1/2/3/4* n=20. All error bars represent mean ± s.d. ****$P \leq 0.0001$; ***$P \leq 0.001$; **$P \leq 0.01$; ns= not significant (*t*-test). All scale bars are 1 μm.

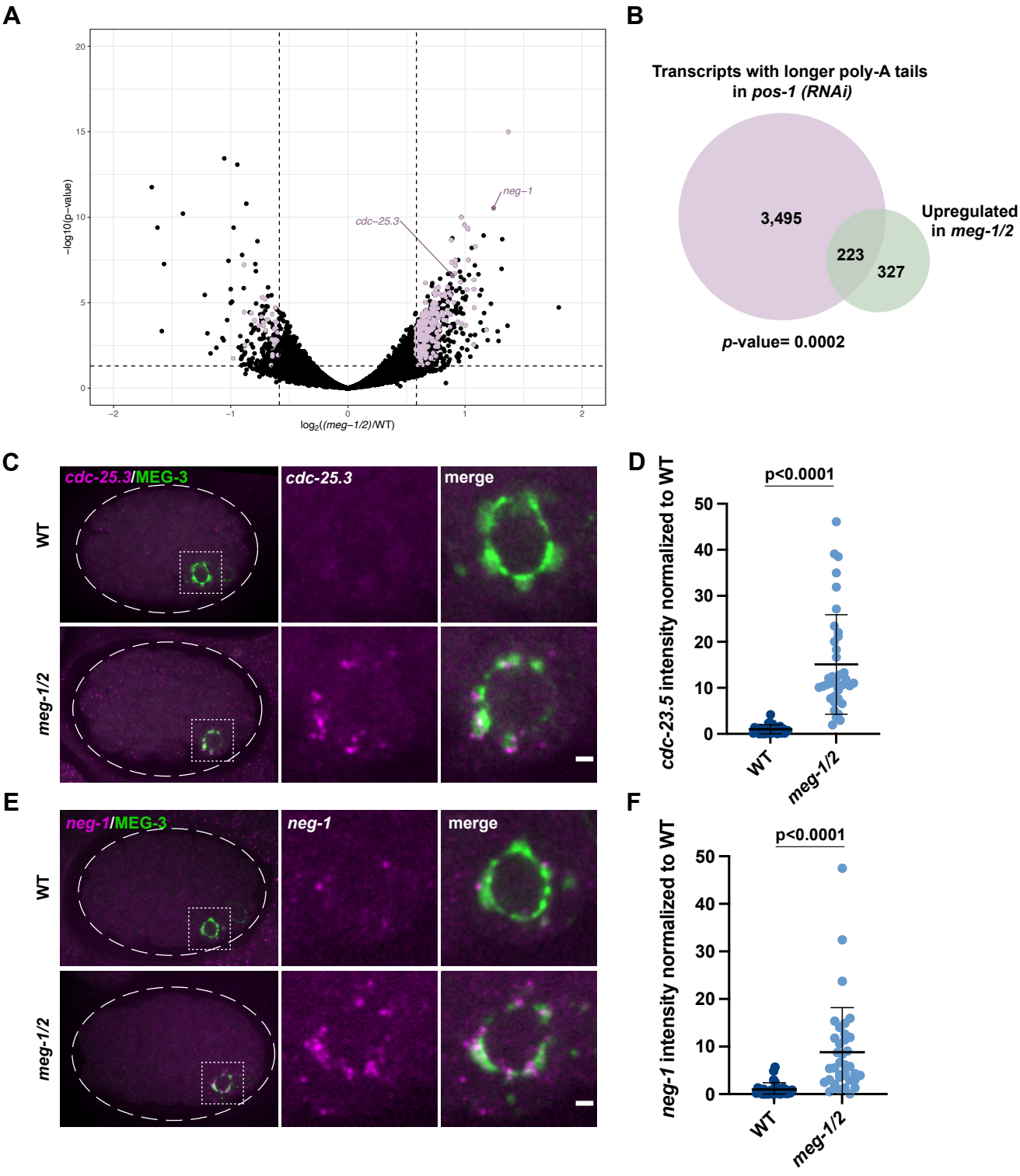

Fig. 5: *meg-1/2* are required for the turnover of a subset of POS-1 targets.
(A) RNA-seq from two independent experiments comparing *meg-1 meg-2* (RNAi) and wild-type embryos identified 230 downregulated and 550 upregulated genes (± 1.5 fold change). Purple dots correspond to genes significantly down/upregulated in *meg-1 meg-2* embryos that also exhibited longer poly-A tails in *pos-1(RNAi)* embryos (Elewa et al., 2015). (B) 223 genes upregulated in *meg-1 meg-2* embryos overlap with genes whose poly-A tails were extended in *pos-1*(RNAi) embryos P=0.0002 (Fisher's exact test, see methods). (C) and (E) Photomicrographs of *cdc-25.3* and *neg-1* smFISH in embryos expressing the P granule marker MEG-3::GFP. Inset shows P_4. *cdc-25.3* and *neg-1* are turned over less efficiently in *meg-1 meg-2* P_4 blastomeres. Scale bars are 1 µm. (D) and (F) Intensity of *cdc-25.3* and *neg-1* in P_4 normalized to wild type. *In situs* for *cdc-25.3* and *neg-1* were done in the same embryos in two independent experiments where mutant and control animals were processed in parallel. Wild type n=29; *meg-1/2* n=38. Error bars represent mean ± s.d. A *t*-test was used to make comparisons between genotypes.

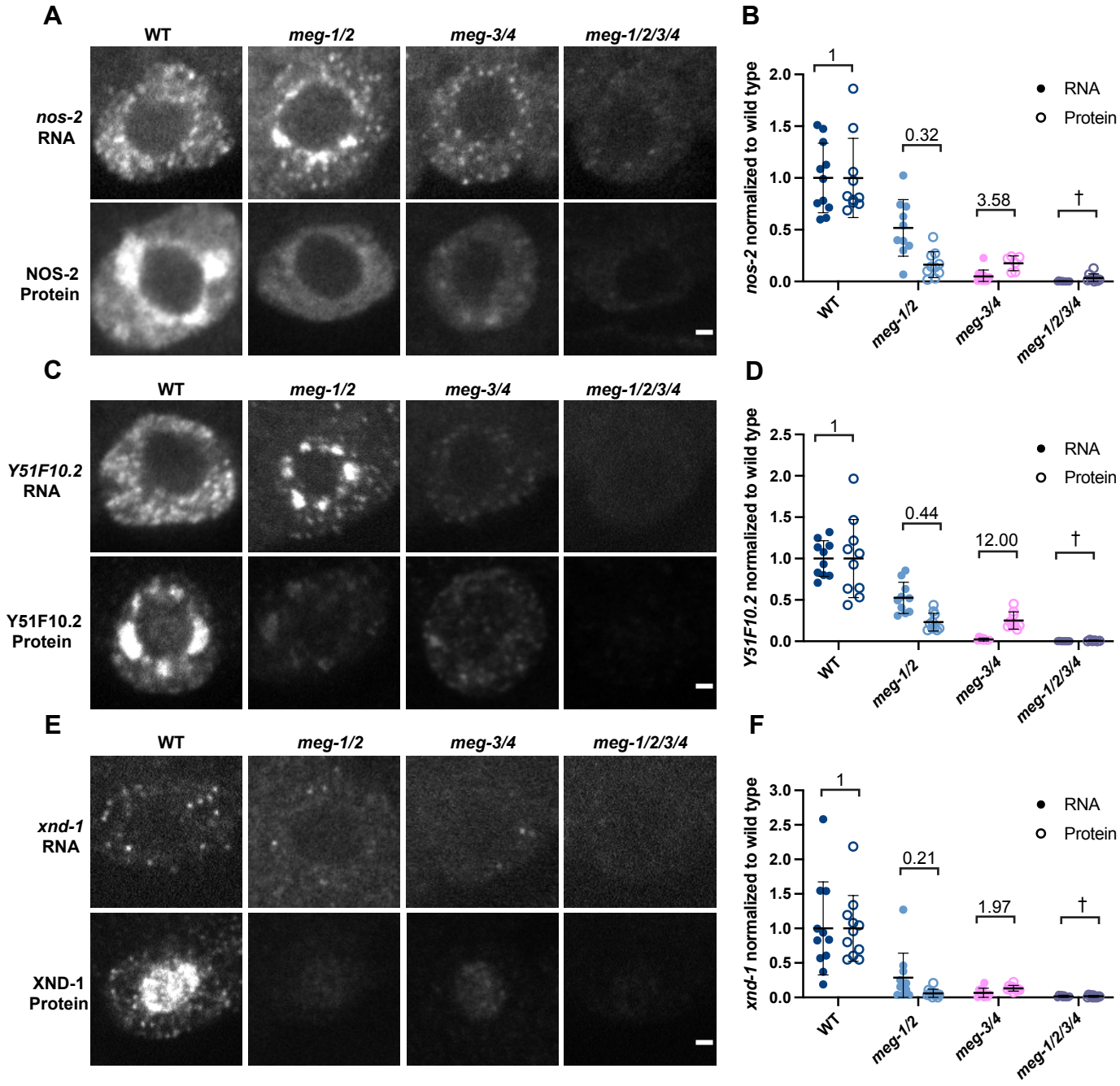

Fig. 6: *meg-1/2* are required for efficient translation of maternal mRNAs coding for germ cell fate determinants.

(A), (C) and (E) Photomicrographs of P_4 in embryos of the indicated genotypes comparing *nos-2, Y51F10.2,* and *xnd-1* RNA and protein levels. In all cases, the RNA is partially reduced in *meg-1 meg-2* mutants, and dramatically reduced in *meg-3 meg-4* and *meg-1 meg-2 meg-3 meg-4*. In contrast, the protein levels of *meg-1 meg-2* and *meg-3 meg-4* are similar. Scale bars are 1 µm. (B), (D) and (F) Intensity of RNA and protein, normalized to wild type. The ratio of protein to RNA levels in each genotype is indicated. In *meg-1 meg-2*, the ratio is decreased, while in *meg-3 meg-4* it is increased. † Due to the very low levels of RNA present in *meg-1 meg-2 meg-3 meg-4* embryos we were unable to calculate the protein/RNA ratio. Quantification for each genotype is from one experiment where mutant and control animals were processed in parallel. For *nos-2* RNA: wild type n=11, *meg-1/2* n=10, *meg-3/4* n=12, *meg-1/2/3/4* n=12. For NOS-2 protein: wild type n=10, *meg-1/2* n=10, *meg-3/4* n=6, *meg-1/2/3/4* n=9. For *Y51F10.2* RNA: wild type n=10, *meg-1/2* n=10, *meg-3/4* n=10, *meg-1/2/3/4* n=9. For *Y51F10.2* protein: wild type n=10, *meg-1/2 n*=10, *meg-3/4* n=9, *meg-1/2/3/4* n=6. For *xnd-1* RNA: wild type n=11, *meg-1/2* n=11, *meg-3/4* n=10, *meg-1/2/3/4* n=10. For XND-1 protein: wild type n=11, *meg-1/2* n=11, *meg-3/4* n=10, *meg-1/2/3/4* n=11. Error bars represent mean ± s.d.

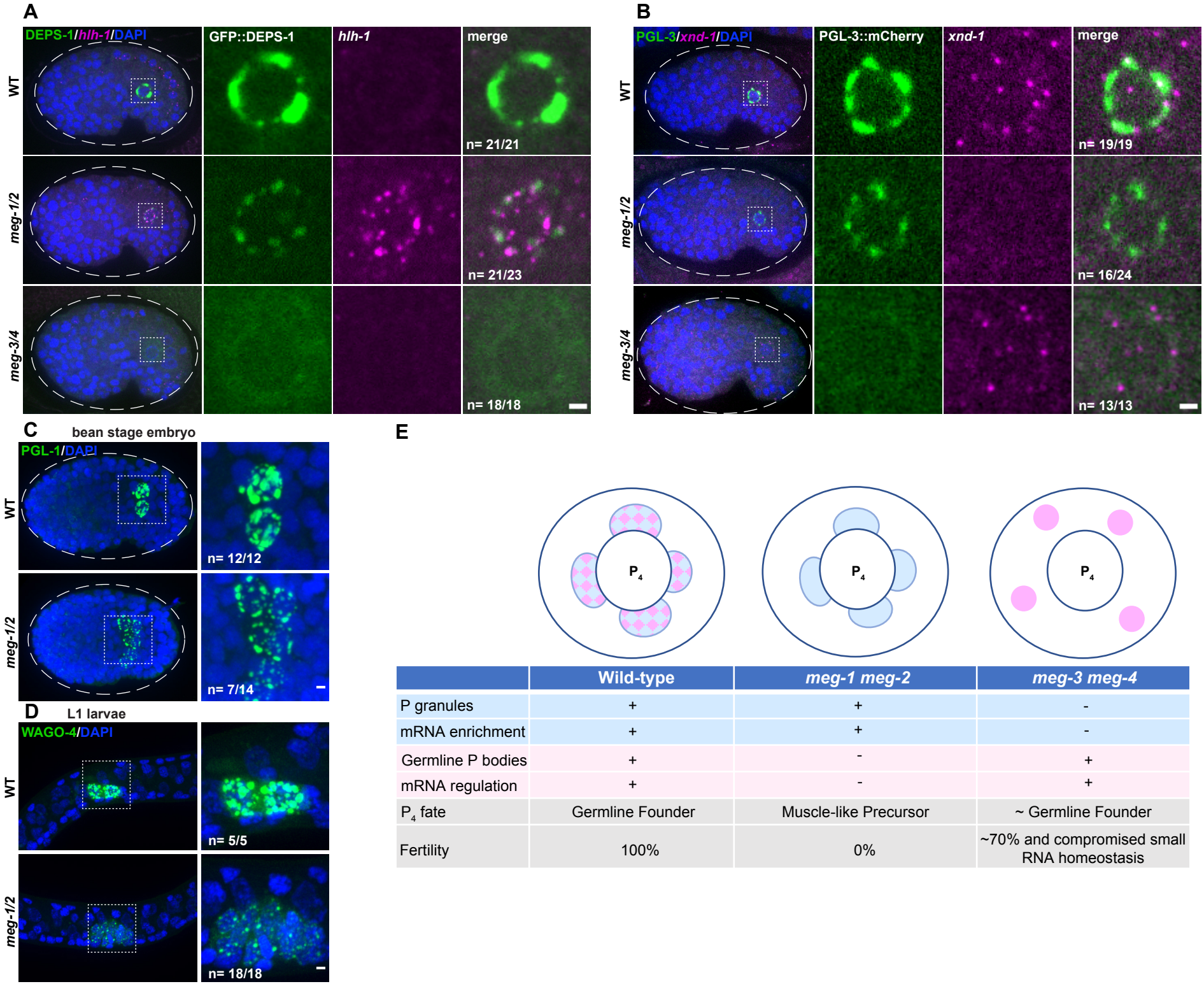

	Wild-type	*meg-1 meg-2*	*meg-3 meg-4*
P granules	+	+	-
mRNA enrichment	+	+	-
Germline P bodies	+	-	+
mRNA regulation	+	-	+
P_4 fate	Germline Founder	Muscle-like Precursor	~ Germline Founder
Fertility	100%	0%	~70% and compromised small RNA homeostasis

Fig.7: Primordial germ cells exhibit somatic-like characteristics in *meg-1 meg-2* mutants.

(A) Photomicrographs of bean stage embryos of the indicated genotypes expressing DEPS-1::GFP and probed for *hlh-1* RNA. Inset depicts a primordial germ cell. Embryos were scored from one independent experiment where mutant and control animals were processed in parallel. 21/21 wild-type and 18/18 *meg-3 meg-4* bean to comma stage embryos did not express *hlh-1*. 21/23 *meg-1 meg-2* did express *hlh-1*. (B) Photomicrographs of bean stage embryos of the indicated genotypes expressing PGL-3::mCherry and probed for *xnd-1* RNA (which is transcribed in PGCs at this stage). Inset depicts a primordial germ cell. Embryos were scored from two independent experiments for *meg-1 meg-2* and one experiment for *meg-3 meg-4* where mutant and control animals were processed in parallel. 19/19 wild-type and 13/13 *meg-3 meg-4* bean stage embryos expressed *xnd-1*. 16/24 *meg-1 meg-2* embryos did not express *xnd-1*. (C) Maximum projections of bean stage embryos of the indicated genotypes stained for PGL-1. Inset shows the primordial germ cells. Embryos were scored from one experiment where mutant and control animals were processed in parallel. 12/12 wild-type embryos had two PGL-1 positive cells and 7/14 *meg-1 meg-2* embryos had more than two PGL-1 positive cells. (D) Maximum projections of germ cells from unfed L1 larvae expressing the germ granule marker 3xFLAG::GFP::WAGO-4. Embryos were scored from one experiment where mutant and control animals were processed in parallel. 5/5 wild-type embryos had two WAGO-4 positive cells and 18/18 *meg-1 meg-2* embryos had more than two WAGO-4 positive cells. All scale bars are 1 μm. (E) Working model: Cartoon and table summarizing P_4 phenotypes based on this study and on Wang et al., 2014 and Ouyang et al., 2019. P granules are depicted in blue, germline P-body in pink, and their merge in a checkered pattern. Note that P granule and germline P-body proteins also exist in a more dilute state in the cytoplasm. See text for additional details.